lubricants

MDPI

Review

A Review of Wear in Additive Manufacturing: Wear Mechanism, Materials, and Process

Xiangjun Jiang [1,*,†], Juntao Lu [1], Na Zhao [2], Zhen Chen [3] and Zhiming Zhao [4]

[1] State Key Laboratory of Electromechanical Integrated Manufacturing of High-Performance Electronic Equipments, Xidian University, Xi'an 710071, China
[2] National Defense Industry Department, China International Engineering Consulting Corporation, Beijing 100089, China
[3] School of Mechanical Engineering, Xi'an Jiaotong University, Xi'an 710049, China
[4] College of Mechanical and Electrical Engineering, Shaanxi University of Science and Technology Xi'an Campus, Xi'an 710600, China
* Correspondence: xjjiang@xidian.edu.cn; Tel.: +86-29-88203115
† Postal Address: School of Mechano-Electronic Engineering, Xidian University, No. 2 South Taibai Road, Xi'an 710071, China.

Abstract: In fields such as industrial engineering and healthcare, additive manufacturing technology is a focal point for researchers. Wear represents a significant challenge for additive manufacturing technology, increasingly emerging as a research hotspot in recent years. This review categorizes and summarizes wear issues in additive manufacturing technology, providing a comprehensive overview of wear mechanisms, materials, and the effects of additive manufacturing processes on wear. Research indicates that different wear mechanisms result in varying wear characteristics. The inherent properties of the materials significantly influence wear during the manufacturing process. Modifying material compositions and optimizing microstructures can enhance the wear properties of additive manufacturing products. Additionally, the study of additive manufacturing technology in repair and maintenance is a current and anticipated research hotspot for the coming decades. In the research of additive manufacturing processes, the effective regulation of process parameters and their post-processing play a positive role in enhancing the wear characteristics of products produced via additive manufacturing. Lastly, the challenges and recent advancements concerning wear issues in the field of additive manufacturing technology research are summarized.

Keywords: additive manufacturing; wear mechanism; material composition; microstructure; process parameter

Citation: Jiang, X.; Lu, J.; Zhao, N.; Chen, Z.; Zhao, Z. A Review of Wear in Additive Manufacturing: Wear Mechanism, Materials, and Process. *Lubricants* **2024**, *12*, 321. https://doi.org/10.3390/lubricants12090321

Received: 23 August 2024
Revised: 10 September 2024
Accepted: 16 September 2024
Published: 17 September 2024

1. Introduction

Additive manufacturing (AM), commonly referred to as 3D printing, is a cutting-edge manufacturing technique that seamlessly integrates computer-aided design, material processing, and forming technologies. Leveraging digital model files, it employs sophisticated software and numerical control systems to precisely layer specialized metal, non-metal, and medical biomaterials through techniques such as extrusion, sintering, melting, photopolymerization, and spraying, ultimately yielding solid objects. This remarkable technology was initially conceptualized by Charles Hull in 1986 through stereolithography (SLA). Over the years, it has evolved to encompass numerous innovative technologies and materials [1].

On the other hand, wear encompasses the dimensional alterations and material depletion that occur at the contact interfaces of materials (components) during their interaction [2]. In the additive manufacturing process, wear issues inevitably arise in materials and additive manufacturing machines. To gain a deeper understanding of the interplay between additive manufacturing and wear, Renner et al. [3] conducted a comprehensive review on the corrosion and wear of additive manufacturing alloys, focusing on several commonly used alloys. Orgeldinger et al. [4] summarized the tribological behavior and surface characteristics of components produced via additive manufacturing. However, these studies

lacked a comprehensive and systematic overview of how material composition design, manufacturing processes, and heat treatment influence wear in additive manufacturing. Therefore, we conducted a review study on the impact of various factors on wear issues in additive manufacturing, aiming to analyze the effects of material composition, microstructure, manufacturing parameters, and heat treatment on wear performance and mechanisms, categorizing and summarizing our findings. We provided insights into the wear issues in additive manufacturing and explored its future developments. This study thus offers interested readers an entry point into the wear research in the additive manufacturing field.

2. Wear Mechanism

Wear mechanisms can take many forms and are categorized into abrasive wear, adhesive wear, fatigue wear, and so on, based on the surface damage characteristics of materials (components). The wear mechanism is influenced by numerous factors, including the material's properties, surface condition, lubrication, contact load, and even environmental temperature and operational conditions. In additive manufacturing, the varying wear mechanisms distinctly impact wear issues.

In the context of additive manufacturing, the wear mechanisms of materials are typically diverse. However, it is possible that some materials may exhibit a single or predominant wear mechanism during the manufacturing process, and research into such issues holds value. Zou et al. [5] analyzed three types of Ti6Al4V samples—those prepared conventionally, via SLM, and by post-heat treatment—and found that their surfaces displayed distinct wear mechanisms when in contact with both soft and hard materials, leading to varied wear characteristics. On the surface of the sample in contact with soft brass, minor brass transfer from the counter material was observed, along with plow marks, adhesive wear, and material transfer. In contact with 38CrMoAl, severe wear, including flaking, oxidative wear, abrasive wear, and deep grooves, was obvious on the surfaces of all three types of samples. However, only the heat-treated selective laser melting (SLM) samples exhibited protective trioxide, with no signs of plastic deformation and the lowest wear rate. The superalloy aluminum-silicon produced via SLM features a unique pseudo-eutectic microstructure, leading to abrasive wear [6]. Heino et al. [7] investigated the tribological behavior of tool steel disks produced via SLM when in contact with aluminum alloy under analogous hot forming conditions. The findings revealed that the primary wear mechanism of AM tool steel is abrasive wear. At 500 °C, the wear debris on the sample surface undergoes further oxidation, compaction, and sintering, resulting in the formation of a smooth glaze layer on the aluminum alloy pin surface, typically correlating with reduced wear rates and lower friction coefficients. Three circular textures (T1, T2, T3) were fabricated on the polylactic acid (PLA) polymer surface using fused deposition modeling [8]. Surface analysis indicated that the wear was primarily due to adhesive wear, with texture T2 exhibiting minimal surface damage at lower speeds and texture T3 displaying the least damage at higher speeds. Shanmugam et al. [9] examined the tribological characteristics of austenitic stainless steel 347 specimens produced via wire arc additive manufacturing (WAAM) under high-temperature, non-lubricated conditions. Detailed analyses of the worn surfaces were conducted using scanning electron microscopy (SEM) and energy-dispersive spectroscopy (EDS). At 200 °C, the worn surfaces of the base material and SLM 347 stainless steel displayed rough plowing features and plastic deformation, with minimal oxide formation. The wear mechanism was adhesive wear. Between 400 and 600 °C, the sample surface displayed shallow grooves, fine oxide particles, and a mechanically mixed composite oxide layer, all contributing to a reduced wear rate. The wear mechanism was mild oxidative wear. Miresmaeili et al. [10] investigated the wear resistance of WAAM stainless steel 347 that underwent deposition and interlayer cold working. The findings revealed that interlayer cold working enhanced the sample's hardness, consequently boosting its wear resistance, with the primary wear mechanism being abrasive wear. Ferreira et al. [11] fabricated 18Ni300 and H13 tool steels using SLM, discovering that H13 steel demonstrated greater wear resistance and a lower wear rate

compared to 18Ni300 steel. The predominant wear mechanisms differed between the two: 18Ni300 steel experienced abrasive cutting, whereas H13 steel suffered from abrasive fatigue wear. A eutectic Al-12Si (wt.%) alloy was fabricated via SLM technology, exhibiting abrasive wear as the wear mechanism, and the eutectic microstructure of the SLM Al-Si alloy was linked to abrasive wear [12]. Surface analysis of the samples revealed that conventionally cast Al-Si alloys displayed significant wear, characterized by pronounced furrows and plastic deformation, whereas the SLM-processed alloys demonstrated comparatively minor signs of wear. Slatter et al. [13] compared the wear resistance of Ti6Al4V alloy produced via traditional methods and electron beam melting (EBM). Samples produced by EBM demonstrated notably inferior wear resistance. Cast samples primarily experience three-body wear, whereas EBM samples exhibit two-body wear. Yadav et al. [14] employed direct energy deposition technology for the additive manufacturing of austenitic stainless steel. The study evaluated the macro- and microstructures, mechanical properties, and wear characteristics in different spatial directions (0°, 90°, and 45°) of the top, middle, and bottom regions of the deposited structures. Wear test results indicated signs of mild oxidation and adhesive wear. Deposition of mechanically mixed composite layers revealed that an increased oxidation percentage facilitated the healing of the worn surface. Using dual-wire arc additive manufacturing technology, functionally graded materials (FGM) comprising SS316LSi and ER70S-6 were deposited. The worn surface of these materials demonstrated adhesive wear. Compared to SS316LSi and ER70S6, the deposited FGM showed superior wear resistance and mechanical properties [15].

However, in additive manufacturing, the wear mechanism is not static but varies with the wear process. Concurrently, the wear characteristics of materials also change accordingly. At a scanning speed of 450 mm/s, the WC/Inconel 718 composite material achieves a low friction coefficient of 0.35 and a wear rate of 2.5×10^{-4} $mm^3/(N \cdot m)$. The surface morphology image reveals the formation of a continuous, hardened friction layer on the worn surface. The wear mechanism varies with different laser scanning speeds, transitioning from predominant abrasive wear to adhesive wear [16]. Pola et al. [17] conducted sliding wear and erosion tests to characterize the AlMgSc alloy produced by direct metal laser sintering (DMLS) under annealed conditions. The wear mechanism transformed from adhesive wear to frictional oxidation wear, which had an impact on the wear rate. Jackson et al. [18] conducted a study on the wear behavior of 17-4PH produced through laser powder bed fusion (L-PBF) technology under both lubricating and dry conditions, subject to external loads of 10 N and 30 N. Their findings revealed that under dry conditions, LB-PBF 17-4PH exhibited a lower wear rate compared to CM 17-4PH. However, under lubricating conditions, the trend reversed, attributed to the shift in wear mechanism from adhesive wear to fatigue wear due to lubrication. Wang et al. [19] employed laser cladding (LC) to deposit a 17-4 PH coating onto 27SiMn steel and subsequently enhanced the coating via laser shock peening (LSP) post-processing at various laser energies. Friction coefficient tests revealed that the base 27SiMn steel had a friction coefficient of 0.704, whereas the LC coating exhibited a lower coefficient of 0.618. Additionally, the wear rate of the coating was markedly reduced, with the wear mechanism transitioning from adhesive wear to predominantly abrasive wear. Dong et al. [20] explored the friction behavior of brake disks under high-speed conditions, observing a substantial friction coefficient. Notably, the friction coefficient decreased due to the low elastic modulus and the presence of third-body friction. Furthermore, as an oxide film formed, the wear mechanism shifted from abrasive wear to adhesive wear. Bai et al. [21] utilized various laser direct energy deposition (L-DED) parameters to achieve two distinct TiC morphologies: equiaxed and dendritic. The findings revealed that the shift from equiaxed to dendritic morphology in titanium matrix composites (TMCs) altered the wear mechanism. The wear scar surface of TMCs with equiaxed TiC displayed pronounced wear grooves, microscopic cracks, and occasional dark spots, indicative of abrasive wear. Conversely, the TMCs with dendritic TiC exhibited dark spots enriched with oxygen at the center of the wear scar, evidencing

oxidative wear. The detachment and fragmentation of equiaxed TiC resulted in a shift from two-body to three-body wear, thereby reducing wear resistance.

On the other hand, wear can also arise from the combined action of multiple wear mechanisms. The SLM-processed Al-50Si (wt.%) sample exhibits a mixed wear mechanism involving abrasive particles and oxidation, with research results proposing a plausible wear process [22]. Utilizing laser additive manufacturing (LAM) technology, Inconel 718 high-temperature alloy achieved its lowest wear rate at a laser power of 1200 W, attributed to abrasive and adhesive wear mechanisms [23]. AlNbTaZrx high-entropy alloy (HEAs) coatings were successfully fabricated on Ti6Al4V via laser cladding [24]. The study revealed that as the content of x varies from 0.2 to 1.0, the wear resistance of the coatings significantly surpasses that of the substrate, with a reduction of approximately 31% in both wear volume and rate. The wear mechanism transforms from micro-cutting (x = 0.2) to a combination of micro-cutting and oxidation (x = 0.4, 0.6, 0.8), ultimately evolving into micro-cutting, oxidation, and brittle debonding (x = 1.0), resulting in the coating with x = 0.8 exhibiting optimal wear resistance. Dangnan et al. [25] discovered that 3D ABS printed samples demonstrated higher wear rates across all pressure loads when compared to Verogray polymer, and this was attributed to abrasive wear mechanisms. Nath et al. [26] conducted a comparative analysis of the wear resistance of L-PBF 15-5 precipitation-hardened (PH) stainless steel against traditionally manufactured aged-formed material (W_H900). In the dry wear test, the material volume loss of the S_H900 sample decreased by 21.45% compared to the W_H900 sample. The primary wear mechanisms observed for 15-5PHSS specimens during room-temperature wear testing were micro-cutting and micro-plowing. Hardell et al. [27] conducted a study on the wear behavior of additively manufactured martensitic aged steel, revealing similar wear mechanisms on the material surface during milling and grinding: adhesive wear, abrasive wear, and delamination wear. Notably, AM martensitic aged steel exhibited slightly superior yet more erratic friction properties compared to traditional aged steel. Kan et al. [28] investigated the sliding wear performance of AlSi10Mg fabricated through L-PBF in comparison with bearing stainless steel. Their findings indicated that the primary wear mechanisms during the wear process were adhesive wear and abrasive wear. Chen et al. [29] examined the 30Cr15MoY alloy steel coating produced by direct laser metal deposition (DLMD) with a laser energy volume density (EVD) of 128 J/mm. This coating exhibited the highest hardness and lowest wear rate, attributed to the combined effects of abrasive wear, adhesive wear, and oxidative wear. Furthermore, at a scanning speed of 700 mm/s, the processed SLM Fe-Mn alloy demonstrated the lowest wear rate, with abrasion and oxidative wear being the primary wear mechanisms [30]. Cam et al. [31] performed boronization on Ni-based Inconel 625 superalloy samples produced via Arc Directed Energy Deposition (Arc-DED). The results indicated that the boronated samples exhibited narrow and shallow wear tracks at room temperature, accompanied by microcracks and localized fractures, with the wear primarily attributed to these microcracks and oxidative wear. At 500 °C, the boronized samples displayed wider wear tracks than at room temperature, a completely smooth surface, and wear residues in some areas, suggesting rapid oxidation of the boronized layer and a shift in the wear mechanism to oxidative wear. Consequently, it is concluded that boronization enhances the wear resistance of Inconel 625 components produced by Arc-DED at both room and high temperatures. Yang et al. [32] explored the application of iron-based, nickel-based, and cobalt-based self-fluxing alloy powders as repair materials in LC technology. The wear mechanisms in the repaired regions of iron-based alloy samples primarily involve adhesive wear, whereas the wear mechanisms in the repaired regions of nickel-based alloy samples are primarily adhesive wear and oxidative wear. Zhang et al. [33] employed multi-wire arc additive manufacturing (MWAAM) to fabricate Ti6Al4V (TC4) and Ti6.5A13.5Mo1.5Zr0.3Si (TC11) alloys, conducting friction coefficient tests (with loads of 20 N and 60 N) and material characterization. The results indicated that at a load of 20 N, the COF values for TC4 and TC11 samples stabilized at 0.479 and 0.455, respectively, whereas at 60 N, these values were 0.472 and 0.432, respectively. Under both load conditions, the COF value for TC11 alloy was lower than

that of TC4, suggesting superior wear resistance in TC11. The wear mechanism for TC4 alloy is a combination of adhesive, oxidative, and delamination wear. For TC11, the wear mechanism is delamination and oxidative wear. Vineesh et al. [34] investigated the sliding wear properties of SS316L, prepared using direct metal laser sintering (DMLS), against chromium steel and alumina. Both materials exhibited a mixed wear mechanism involving oxidation, abrasive particles, and adhesion. Notably, alumina undergoes delamination wear at higher temperatures. Herranz et al. [35] conducted a study comparing 17-4PH stainless steel samples and fuse-manufactured samples produced via SLM with traditional forged steel samples. Notably, under all experimental conditions, AM 17-4PHSS exhibited a lower wear rate and friction coefficient, with the primary wear mechanism attributed to the formation of an iron/chromium oxide film and delamination wear. Cui et al. [36] utilized LC technology to fabricate a FeCoCrNi2MoSi eutectic high-entropy alloy coating. At ambient temperatures, the coating's worn surface displayed significant debris and extensive grooves aligned with the sliding direction, characterized by adhesive and abrasive wear. With increasing temperatures, the wear mechanism transitioned predominantly to oxidative and delamination wear. At 800 °C, an oxide layer formed on the worn surface, mitigating direct contact and acting as a lubricant, leading to the minimum wear rate at this temperature. Furthermore, research on depositing composite coatings with varying SiC contents onto TC4 surfaces using LC technology revealed that the coatings' primary wear mechanisms were a complex interplay of adhesive, abrasive, and oxidative wear, whereas the TC4 substrate primarily exhibited micro-cutting wear [37]. Significantly, the composite coatings were found to enhance the hardness and wear resistance of the TC4 substrate.

A comprehensive review of the latest literature underscores the significant impact of both singular and mixed wear mechanisms on the wear characteristics of additive manufacturing products. This section summarizes the experimental equipment and methods used in the friction and wear experiments and micro-scratch surface morphology collected in our literature review, as shown in Table 1. Understanding these mechanisms is crucial for identifying the primary types of wear and implementing targeted measures to mitigate wear effectively.

Table 1. Overview of experimental research on additive manufacturing materials.

Additive Technology	Experimental Subjects	Experimental Equipment	Experimental Methods	Research Findings	Reference
SLM	Ti6Al4V	Ring-on-disk rig	X-ray diffraction (XRD), scanning electron microscopy (SEM), energy-dispersive X-ray spectroscopy (EDS), confocal laser scanning microscopy (CLSM), optic microscopy (OM)	A small amount of brass was observed to transfer from the counter-material on the surface of the sample in contact with soft brass, with plow marks, adhesive wear, and material transfer on the surface. When in contact with 38CrMoAl, severe wear can be observed on the sample surface, including spalling, oxidative wear, abrasive wear, and deep grooves.	[5]
SLM	Hypereutectic Al-Si alloy	Ball-on-disk wear test	XRD, OM, SEM	SLM Al-18Si and Al-50Si alloys exhibit similar friction coefficients of approximately 0.4. The wear rate of Al-18Si is slightly higher than that of Al-50Si sample. And the SLM-processed hypereutectic Al-Si alloy exhibits higher wear resistance than the conventionally cast sample.	[6]
SLM	Chisel tool steel	Pin-on-disk tests	SEM, EDS	A constant sliding speed, normal load, and temperature were maintained during the experiment while recording the friction coefficient online. At 500 °C, wear debris forms a smooth glaze layer on the surface of the aluminum alloy pin, which helps to reduce the friction coefficient and improve wear resistance.	[7]
Fused deposition modeling technique	Polylactic acid (PLA) polymer	Pin-on-disk tribometer	SEM	Texture T2 exhibits the lowest friction coefficient under dry conditions, while under lubricated conditions, texture T3 exhibits the lowest friction coefficient at low speeds, and texture T1 exhibits the lowest friction coefficient at high speeds. Surface texture reduces friction coefficient by reducing contact area and retaining lubricant, but texture size and sliding speed have a significant impact on lubricant retention ability and friction coefficient.	[8]

Table 1. *Cont.*

Additive Technology	Experimental Subjects	Experimental Equipment	Experimental Methods	Research Findings	Reference
SLM	Austenitic stainless steel 347	Pin-on-disk tribometer	EDS, electron backscattered diffraction (EBSD) SEM, XRD	At 200 °C, the worn surfaces of the substrate and SLM 347 stainless steel exhibit rough plowing features and plastic deformation, as well as minimal oxide formation. At 400–600 °C, there are some shallow grooves and small oxide particles on the surface of the sample, as well as a mechanically mixed composite oxide layer, which reduces the wear rate.	[9]
WAAM	Stainless steel 347	Pin-on-disk wear tests	SEM, EDS	Cold working treatment (CW) increased the hardness of the sample, thereby improving wear resistance and reducing friction coefficient.	[10]
SLM	18Ni300 and H13 tool steel	Pin-on-disk apparatus	SEM, EDS, XRD	The wear rate of H13 steel is two orders of magnitude lower than that of 18Ni300 steel (H13 is 0.11×10^{-7} $mm^3/(N{\cdot}m)$, and 18Ni300 is 18.44×10^{-7} $mm^3/(N{\cdot}m)$). Compared with 18Ni300 steel, the wear trajectory of H13 steel is deeper and wider.	[11]
SLM	Al-12Si alloy	Ball-on-disk contact sliding test	SEM, EDS, OM, EBSD, transmission electron microscope (TEM)	Traditionally cast Al-Si alloys exhibit severe wear, with obvious plowing and plastic deformation characteristics, while SLM-treated alloys show milder wear marks.	[12]
EBM	Ti6Al4V	Dry-sand–rubber wheel-type abrasive wear test apparatus	SEM	The wear volume of EBM samples is significantly larger than that of conventional samples, and their wear rate is 120% higher than that of conventional samples. The wear scars of all samples showed three-body wear and plowing phenomenon.	[13]
DED	Austenitic stainless steel	Tribometer (MFT-5000)	SEM, EDS	Under loads of 20 N, 25 N, and 30 N, the COF values of the samples ranged from 0.5410 to 0.5688, with the lowest (25.9×10^{-4} $mm^3/(N{\cdot}m)$) and highest (39.6×10^{-4} $mm^3/(N{\cdot}m)$) observed wear rates.	[14]
Twin wire arc additive manufacturing technique	FGM	Multifunctional tribometer	SEM, EDS, XRD	The chemical composition analysis of different areas on the worn surface of the sample shows a significant increase in oxygen content, indicating the existence of an adhesive wear mechanism during the wear process. Simultaneously observing particles of different sizes and rich in oxygen indicates the dominant role of the adhesive wear mechanism in the sample.	[15]
SLM	WC/Inconel 718	Ball-on-disk tribometer	SEM, EDS, OM	When the scanning speed was 450 mm/s, SLM WC/Inconel 718 composite material achieved a low friction coefficient (0.35) and a wear rate of 2.5×10^{-4} $mm^3/(N \cdot m)$. The wear mechanism changed under different laser scanning speeds, gradually transitioning from severe abrasive wear to adhesive wear.	[16]
DMLS	AlMgSc alloy	Pin-on-disk test, a 100Cr6 steel ball with a 6 mm diameter	SEM, EDS	As the sliding distance increases, the friction coefficient gradually decreases, and wear fragments and parallel grooves can be seen in the wear trajectory, as well as plow grooves formed by the drag of oxide particles. The wear mechanism changes from adhesive wear to frictional oxidation wear.	[17]
L-PBF	17-4 PH coating	Ball-on-disk wear test, high carbon chrome steel balls with a diameter of 10 mm	SEM	Both LB-PBF and CM (traditional manufacturing) samples exhibit lower friction coefficients under lubricated conditions compared to dry conditions.	[18]
LC	17-4 PH coating	MS-T3001 ball–disk wear tester, GCr15 steel with a diameter of 6 mm	OM, SEM, EBSD, TEM	The friction coefficient of the 27SiMn steel matrix material is 0.704, while the friction coefficient of the LC coating is relatively low at 0.618, and the wear rate of the coating is significantly reduced. The wear mechanism changes from adhesive wear to slight abrasive wear.	[19]
SLM	Brake disks	Full-scale flywheel brake dynamometer	—	Compared to cast brake disks, SLM brake disks have a more stable friction coefficient, shorter braking distance, and higher braking energy efficiency under high-speed conditions. As the temperature increases, the wear mechanism of the sample shifts from abrasive wear to adhesive wear.	[20]
L-DED	TMCs	Ball-on-flat reciprocating tribometer, WC balls	XRD, EDS, SEM, TEM	Obvious wear grooves, microscopic cracks, and a small amount of dark spots were observed on the surface of the TMC wear track of equiaxed TiC, indicating that abrasive wear occurred. However, a dark spot rich in oxygen elements was observed at the center of the TMC wear track of dendritic TiC, indicating the presence of oxidative wear.	[21]

Table 1. *Cont.*

Additive Technology	Experimental Subjects	Experimental Equipment	Experimental Methods	Research Findings	Reference
SLM	Al-50Si alloy	Unlubricated ball-on-disk wear test, 3 mm diameter Al_2O_3 ball	SEM, XRD, EDS	At a sliding distance of 125 m, the average friction coefficients of the 275 W, 320 W, and 350 W samples were 0.51, 0.49, and 0.48, respectively. The wear mechanism of SLM high-silicon aluminum alloy is different from that of conventional casting alloys, which is abrasive wear and oxidative wear.	[22]
LAM	Inconel 718	MDW-02 reciprocating friction and wear tester, 3 mm diameter bearing steel GCr15 ball	XRD, SEM, EDS, OM	Appropriate laser power can help improve the wear resistance of materials. At a laser power of 1200 W, the material exhibited the best wear performance, with the smallest fluctuation in friction coefficient and wear rate. The wear mechanism remains unchanged with variations in laser power, consistently comprising a combination of abrasive and adhesive wear, although there are notable differences in the extent of wear.	[23]
LC	$AlNbTaZr_x$ HEA coatings	CFT-1 ultra-functional wear-test machine, 5 mm diameter hard Si_3N_4 ceramic balls	SEM, EDS, X-ray photoelectron spectrometer (XPS)	Compared with the substrate, the average wear volume and wear rate of the coating were reduced by about 31%. The worn surface of the substrate is very rough, with many grooves roughly parallel to the sliding direction, indicating severe micro-cutting wear.	[24]
Polyjet	ABS, Verogray polymer	Bruker Universal Material Test	SEM	Compared with Verogray polymer, the 3D ABS printed sample exhibited a higher wear rate under all pressure loads, which is attributed to the abrasive wear mechanism.	[25]
L-PBF	15-5 PH stainless steel	DUCOM High-Temperature Dry Abrasion tester	SEM, EBSD	The three-body dry wear test conducted at room temperature and high temperature (300 °C) showed that the wear volume loss of the L-PBF sample (S_H900) was significantly lower than that of the forging sample (W_H900). The main wear mechanisms are micro-cutting and micro-ploughing.	[26]
SLM	Maraging steel	Hot-strip drawing tribometer	SEM, EDS	The friction behavior of SLM maraging steel at high temperatures is mainly controlled by the formation of a FeAlSi intermetallic compound transfer layer. The wear mechanism of the sample during the wear process is mainly adhesive wear and abrasive wear.	[27]
L-PBF	AlSi10Mg alloy	Pin-on-disk tests	EBSD, SEM, EDS, OM	In contact with stainless steel, the wear track is mainly composed of parallel grooves, indicating the presence of abrasive wear.	[28]
DLMD	30Cr15MoY alloy steel coating	MFT-5000 wear test machine	SEM, EDS, XRD, TEM, EBSD	The friction coefficient of all samples increased from 0 to about 0.6, and then the friction coefficient increased slowly, showing a sawtooth pattern. When EVD is 128 J/mm^3, the sample has the lowest wear rate (6.49×10^{-6} $mm^3/(N{\cdot}mm)$). The wear mechanism is a combination of abrasive wear, adhesive wear, and oxidative wear.	[29]
SLM	Fe-Mn alloy	Ball-on-disk tribometer	SEM, EDS, XRD, TEM	The sample with the lowest microhardness exhibits the lowest friction coefficient and excellent friction and wear properties. The wear mechanism of Fe-Mn alloy mainly includes abrasive wear and oxidative wear, while pure iron mainly exhibits adhesive wear.	[30]
Arc-DED	Inconel 625	Dry sliding ball-on-disk wear tests	XRD, SEM, EDS	The wear resistance of Inconel 625 parts manufactured by Arc-DED at room temperature and high temperature through boronization was improved.	[31]
LC	Self-fluxing alloy powders	HT-1000 ball–disk wear tester	OM, SEM, EDS	During the stable phase, the Co-based alloy coating sample exhibited the lowest friction coefficient, approximately 0.41. The friction coefficients of Fe-based and Ni-based alloy repair coating samples were stable at 0.63 and 0.75, respectively. Co-based alloy coating exhibits the best wear resistance under high-temperature wear conditions.	[32]
MWAAM	TC4 alloy, TC11 alloy	Bruker UMT-5 friction tester	XRD, EBSD, OM, SEM, EDS	The COF value of TC11 alloy is lower than that of TC4 alloy under both loading conditions, indicating that TC11 alloy has better wear resistance.	[33]
DMLS	Stainless steel 316L	High-frequency reciprocating tribometer	EBSD, SEM, XRD, EDS	DMLS 316L stainless steel exhibits good wear resistance under high-temperature dry sliding wear conditions, especially at 200 °C, where its wear resistance is significantly improved due to the formation of a surface oxide layer. However, at higher temperatures, the wear rate increases due to the destruction of the oxide layer and the softening of the material.	[34]

Table 1. *Cont.*

Additive Technology	Experimental Subjects	Experimental Equipment	Experimental Methods	Research Findings	Reference
SLM	17-4 PH stainless steel	Pin-on-disk, ball-on-plate and lubricated pin-on-disk wear test	SEM, EDS	The friction coefficient (COF) of all samples under lubricated conditions is lower than that under dry friction conditions. After wear, the width of the wear scar of all samples under lubrication conditions is smaller than that under dry conditions.	[35]
LC	$FeCoCrNi_2MoSi$ eutectic high-entropy alloy coatings	HT-1000 high-temperature friction and wear tester	XRD, SEM, high-resolution transmission electron microscopy (HRTEM), scanning transmission electron microscopy (STEM), XPS	The friction coefficient decreases from 0.43 at room temperature to 0.20 at 800 °C. The wear rate decreases from 3.92×10^{-5} $mm^3/(N{\cdot}m)$ at room temperature to 1.09×10^{-5} $mm^3/(N{\cdot}m)$ at 800 °C.	[36]
LC	Ti6Al4V, SiC composite coating	HSR-2T high-speed reciprocating friction tester	XRD, EDS, SEM	The average friction coefficient of the composite coating increases with the increase in SiC content, from 1.2 for the 10% SiC coating to 1.6 for the 30% SiC coating. The wear mechanisms of the composite coating mainly include adhesive wear, abrasive wear, and oxidative wear, while the main wear mechanism of the TC4 substrate is micro-cutting.	[37]

3. Wear in Additive Manufacturing Materials

3.1. The Impact of Changes in Material Composition on Wear

In additive manufacturing, alterations in material composition, encompassing the introduction of novel elements or materials, variations in the concentration of identical materials, and the concurrent occurrence of both, exert a significant influence on wear characteristics. This review encompasses a comprehensive compilation of 16 research articles that delve into the impact of material composition modifications on wear in additive manufacturing, summarized in Table 2. The subsequent paragraphs offer a concise overview of the research findings about the effects of material variations on wear performance in additive manufacturing, categorized based on distinct additive elements.

Table 2. The impact of changes in material composition on wear.

Additive Objects	Additive Technology	Added Materials (Elements)	The Impact on Wear	Reason	Reference
Al-15Si alloy	SLM	TiC	Improve wear resistance	TiC has high elastic modulus, high hardness, and other characteristics, and the introduction of TiC improves the wear resistance of the product.	[38]
Inconel 625 alloy	SLM	TiC	Improve wear resistance	TiC particles are uniformly distributed in the alloy matrix and can withstand large loads during wear, dispersing contact stress and reducing direct wear of the matrix material.	[39]
High-chromium white iron	L-DED	Ti TiC	Improve wear resistance	The addition of Ti promotes the formation of in situ TiC and its uniform distribution in the microstructure, which helps to improve the wear resistance. The addition of TiC increases the fraction of carbides, thereby improving the wear resistance.	[40]
Hastelloy X alloy	L-PBF	TiC	Reduce wear rate	TiC nanoparticles inhibit the formation of cracks, effectively resist the penetration of abrasive particles, reduce plastic deformation, and thereby reduce the wear rate.	[41]
Ni60	LC	WC	Improve wear resistance	The addition of WC can effectively improve the surface hardness of the coating, which helps to resist plastic deformation and material loss during wear. At the same time, as the mass fraction of WC increases, the W-containing carbides in the coating increase, which helps to improve the wear resistance of the coating.	[42]
AlSi10Mg	SLM	WC	Reduce wear rate	The introduction of WC particles promotes grain refinement, and as a second phase, WC particles contribute to improving the hardness and wear resistance of materials through dispersion-strengthening and grain-boundary-strengthening mechanisms.	[43]
NiCrBSi	PTA-AM	WC	Improve wear resistance	A more uniform distribution of WC and the formation of complex carbides caused by the thermal degradation of WC in the matrix can improve the wear resistance of the material.	[44]
Ti6Al4V	DMLS	TiB_2	Improve wear resistance	TiB_2 as a reinforcing phase increases the hardness of the material and improves its wear resistance. The addition of TiB_2 promotes the formation of α-Ti and β-Ti phases with good wear resistance. At the same time, it promotes the refinement of grain size, increasing the hardness and wear resistance of the material.	[45]

Table 2. *Cont.*

Additive Objects	Additive Technology	Added Materials (Elements)	The Impact on Wear	Reason	Reference
Ti6Al4V titanium-based ceramic coating	LC	CeO_2	Improve wear resistance	The addition of CeO_2 nanoparticles results in finer and more uniform grains in the coating, which improves the strength and toughness of the material. Grain refinement increases the number of grain boundaries, thereby improving the hardness and wear resistance of the material.	[46]
Ti6Al4V	μ-PAAM	Cr Ni	Reduce wear volume, wear rate, and wear scar depth	The addition of Cr or Ni can refine the grain of the α-Ti phase, which improves the strength and hardness of the material, and the formation of hard intermetallic phases helps to improve the wear resistance of the alloy.	[47]
Al-18Si Al-50Si	SLM	Si	Improve wear resistance	The fine and evenly distributed primary silicon phase exhibits higher wear and corrosion resistance. As the silicon content increases, the size of the primary silicon phase slightly increases, and the presence of the primary silicon phase can resist wear.	[6]
Al	Cold spray technology	Diamond	Improve wear resistance	By utilizing the high hardness characteristics of diamond and the metallurgical bonding mechanism during cold spraying, while using diamond particles as a hard phase, direct contact and friction are reduced during wear, thereby improving the wear resistance of the material.	[48]
Stainless steel	L-PBF	SiC	Reduce wear rate	The addition of SiC affects the grain orientation and refines the grain size, thereby improving the hardness and strength of the material, which helps to improve the wear resistance.	[49]
HiMnMeCr HiMn coating	WAAM	Cr	Affects wear rate and trajectory	The addition of Cr causes the internal structure of the high-manganese steel coating to change from dual-phase austenite + martensite to single austenite while extending the break-in period of the wear process. Due to the work hardening effect caused by severe plastic deformation of austenite, the wear resistance of the high-manganese steel coating is reduced.	[50]
T15 alloy steel coating	PPLC	Cr	Improve wear resistance	The increase in Cr content affects the content of γ-Fe and α-Fe in the coating. The reduction in austenite and the increase in martensite contribute to the improvement of wear resistance.	[51]
High-chromium white iron	DED	B	Reduce wear volume	The addition of B promotes the formation of hard phases, increases the hardness of the material, and helps reduce the volume loss in high-stress wear testing, thereby improving the wear resistance.	[52]

The incorporation of new elements or materials alters the microstructure and mechanical properties of materials produced via additive manufacturing, subsequently influencing their wear characteristics. According to the existing literature, the application of additive manufacturing techniques to incorporate Ti and TiC into materials enhances their wear resistance. Introducing 5 wt.% TiC to the Al-15Si alloy during the SLM process, followed by annealing, enhances the material's plasticity and the adhesion between TiC particles and the matrix, thus boosting its wear resistance. This approach represents a viable method for achieving high microhardness and superior wear resistance [38]. Yan et al. [39] explored the reinforcement of Inconel 625 alloy materials fabricated using SLM technology with varying mass fractions of TiC. They compared the friction and wear properties of samples containing 4 wt.% and 8 wt.% TiC. The findings revealed that as the TiC content increased, the average width and depth of wear marks decreased, indicating improved wear resistance. Notably, the 8 wt.% TiC sample exhibited the best wear resistance, with the lowest average wear mark width (1.05 mm) and the lowest average wear rate ($9.8 \times 10^{-5} mm^3/(N \cdot m)$). Easton et al. [40] incorporated Ti and TiC powders to enhance the wear resistance of L-DEDed high-chromium white iron. The findings revealed that Ti addition facilitated the formation of in situ TiC, which was uniformly distributed within the microstructure, thereby boosting wear resistance, with the sample containing 6.55 wt.% Ti powder exhibiting the best wear performance. The inclusion of TiC led to the deposition of coarser extrinsic TiC and finer in situ TiC within the microstructure, elevating the carbide content and enhancing wear resistance under high-stress conditions. In the needle–disk wear test, the alloy with added TiC powder outperformed the cast sample. HastelloyX alloy, prepared via L-PBF technology, was strengthened by incorporating 3 wt.% nano-TiC

particles [41]. The research demonstrates that the inclusion of 3 wt.% nano-TiC particles effectively enhances the wear resistance of the material. Specifically, under identical forming parameters, the wear rate of the composite material is reduced by 51% compared to pure HastelloyX alloy, achieving a rate of merely 174.49 $\mu m^3/(N \cdot mm)$.

Apart from exploring the wear properties of materials with the addition of Ti and TiC, notable advancements have also been made in studying the incorporation of WC into additive manufacturing materials. Yang et al. [42] discovered that an increase in WC content leads to the formation of a wider variety of W-containing carbides within Ni60/WC composites, thereby significantly bolstering their hardness and wear resistance. Nano-WC/AlSi10Mg composite materials with varying WC contents were fabricated using SLM technology. Compared to other WC/AlSi10Mg composite materials, the 3% WC/AlSi10Mg sample produced via SLM exhibits the lowest average friction coefficient and wear rate. This is attributed to the introduction of WC particles, which facilitate grain refinement. Additionally, serving as a second phase, WC particles enhance the material's hardness and wear resistance through the mechanisms of dispersion strengthening and grain boundary strengthening [43]. Additionally, Rose et al. [44] employed plasma transferred arc additive manufacturing (PTA-AM) to deposit metal matrix composite materials consisting of 60 wt.%, 70 wt.%, and 80 wt.% WC-NiCrBSi. The results reveal that the wear and impact resistance of the 60 wt.%, 70 wt.%, and 80 wt.% PTA-AM samples are comparable to that of the 60 wt.% sample coating.

The remaining summarized literature focuses on the research findings regarding the impact of modifications in other materials on the wear performance of various materials. This includes the preparation of Ti6Al4V alloy with varying concentrations of TiB_2 utilizing direct metal laser sintering (DMLS) technology [45]. Research indicates that as grain size is refined and hardness is altered, the hardness and wear resistance of the Ti6Al4V alloy are progressively enhanced. Furthermore, titanium ceramic coatings were fabricated on Ti6Al4V substrates using TiCN+SiO_2 mixed powders with and without CeO_2 nanoparticles [46]. The incorporation of CeO_2 nanoparticles notably enhanced the coatings' wear resistance under SBF wear test conditions. Jain et al. [47] investigated the incorporation of chromium or nickel into Ti6Al4V alloy and fabricated Ti6Al4V5Cr, Ti6Al4V2.5Cr2.5Ni, and Ti6Al4V5Ni alloys using the μ-plasma arc additive manufacturing process (μ-PAAM). Their research revealed that the addition of chromium or nickel contributes to improving the microhardness of the materials, subsequently reducing wear properties such as friction coefficient, wear volume, and wear rate. Kang et al. [6] examined the tribological effects of 18 wt.% and 50 wt.% silicon contents on supercrystalline aluminum-silicon alloys produced via SLM. Their findings indicate that both Al-18Si and Al-50Si alloys exhibit superior wear resistance compared to traditional cast samples. Xie et al. [48] utilized diamond powder with a core-shell structure to fabricate a series of Al/diamond composites through solid-state cold spray additive manufacturing technology. Wear tests demonstrated that Al/diamond composite materials exhibit superior wear resistance compared to Inconel 625 and 17-4PH alloys. Furthermore, an increase in diamond content within the composite material results in enhanced wear resistance. Tan et al. [49] discovered that the incorporation of SiC significantly enhanced the strength and tribological properties of 316L stainless steel fabricated through L-PBF additive manufacturing technology. Notably, the 316L alloy reinforced with 9 vol% silicon carbide exhibited a remarkably low wear rate of 0.77×10^{-5} $mm^3/(N \cdot m)$, thus achieving the highest wear resistance. Liu et al. [50] fabricated high-manganese and high-manganese-chromium coatings using WAAM, examining the impact of Cr addition on wear performance through sliding wear tests and electrochemical experiments. The study revealed that incorporating Cr transformed the internal structure of the high-manganese steel coating from a dual-phase of austenite and martensite to solely austenite and also lengthened the wear process's break-in period. The severe plastic deformation of austenite led to a work-hardening effect, thereby diminishing the high-manganese steel coating's wear resistance. Furthermore, T15 alloy steel coatings with varying Cr concentrations were produced using pre-set powder laser cladding

(PPLC) [51]. The findings indicated that as the Cr content increased, the wear resistance decreased, with the T15 alloy steel coating containing 10.04% Cr exhibiting the optimal wear resistance. Easton et al. [52] discovered that in two wear tests, the high-chromium white iron alloy containing 1.6 wt.% B exhibited superior wear resistance compared to the cast alloy. In comparison to L-DED high-chromium white iron, the incorporation of B facilitates the formation of hard phases, enhances the material's hardness, and augments the alloy's wear resistance in high-stress abrasive particle tests.

Overall, in the additive manufacturing process, the introduction of new materials (elements) or varying concentrations of the same material significantly impacts the wear resistance of AM materials. For instance, it was indicated in [39] that the 8 wt.% TiC-SLM Inconel 625 alloy exhibits the best wear resistance, with an average wear scar width of 1.05 mm and an average wear rate of 9.8×10^{-5} $mm^3/(N \cdot m)$. However, Hu et al. [41] revealed that incorporating 3 wt.%nano-TiC particles reduces the wear rate of HastelloyX alloy by 51% compared to pure HastelloyX, to just 174.49 $\mu m^3/(N \cdot mm)$. The research in [49] found that 9 vol% SiC-reinforced 316L achieved a notably low wear rate of 0.77×10^{-5} $mm^3/(N \cdot m)$. Therefore, adjusting the material composition emerges as a viable approach to minimize wear and tear and reduce the wear rate in additive manufacturing.

3.2. The Influence of Material Microstructure on Wear

During the additive manufacturing process, the microstructure of materials plays a pivotal role in determining their wear performance. Key influencing factors include grain size and morphology, phase composition, porosity, residual stress, and texture. Microstructure primarily influences the mechanical properties of the materials, such as strength, hardness, and toughness, which subsequently impact their wear rate and wear resistance.

A promising aspect lies in optimizing the microstructure of additive manufacturing materials by adjusting grain morphology to enhance mechanical properties. Further research is imperative in this domain to ascertain methods for developing ideal microstructures [53]. Under lubricating conditions, 316L stainless steel was fabricated using both SLM and traditional methods [54]. The research reveals that the friction and wear characteristics of SLM samples in contact with brass are marginally superior to those of traditionally processed samples, attributed to the increased wear resistance conferred by the refined grains within SLM samples. Nevertheless, upon contact with harder materials, the samples undergo significant plastic deformation. Due to the presence of refined particles in their microstructure, the tribological properties of SLM samples are anticipated to outperform those of traditionally processed samples. Zou et al. [5] prepared three varieties of Ti6Al4V samples: those prepared through conventional treatment, those fabricated using SLM, and SLM samples subjected to heat treatment. The findings indicate that these three types of samples exhibit distinct microstructures and wear behaviors. Among the three distinct processing techniques utilized for fabricating austenitic 316L stainless steel, namely SLM, hot pressing, and conventional casting, the SLM-prepared variant exhibits a finer microstructure and superior wear resistance [55]. Yu et al. [56] successfully fabricated AlSi10Mg nanocomposites reinforced with 0.5% carbon nanotubes by leveraging SLM technology. Their findings reveal that the reinforcement of carbon nanotubes leads to enhanced surface hardness and a unique layered microstructure in the nanocomposites, thereby improving their wear resistance. Jeyaprakash et al. [57] developed SS304 samples using SLM technology and compared them with traditionally cast samples. Notably, the SLM samples exhibited an ultrafine grain microstructure on their surface, resulting in a significant enhancement in wear resistance. Hemachandra et al. [58] discovered that the SLM Al-Si alloy possesses superior wear resistance due to the formation of a unique particle eutectic microstructure resulting from the high cooling rates during the SLM process. The rapid formation of a nanocrystalline layer within the microstructure of the Ag coating after additive manufacturing effectively mitigates the downward penetration of shear stress and strain, demonstrating the superior wear resistance of the processed Ag coating [59] (Figure 1). In contrast to traditional manufacturing techniques, the topmost layer of the worn surface of the nickel-based single-crystal (NBSC) high-temperature alloy

SRR99, fabricated through laser-directed energy deposition (L-DED), has undergone notable plastic deformation and microstructural alterations. This results in the formation of a graded microstructure, thereby enhancing compactness, minimizing debris formation, and safeguarding against long-term wear damage [60].

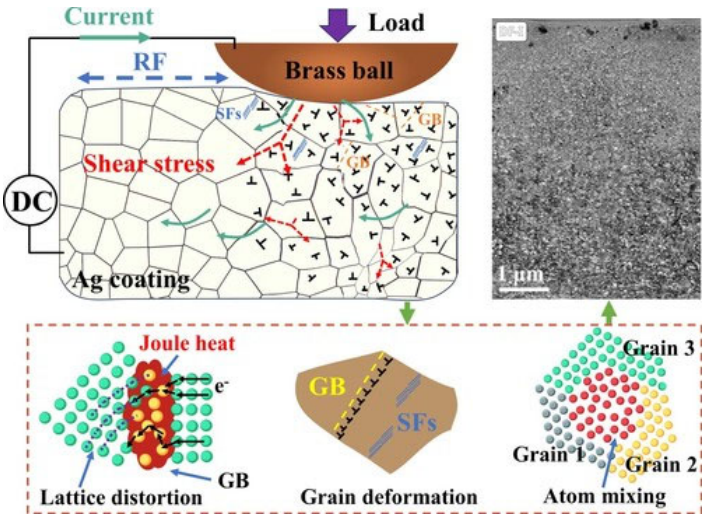

Figure 1. Schematic diagram of microstructure evolution mechanism of silver coating through current-carrying friction [59].

Smaller grain size and uniform phase composition can enhance the strength and hardness of materials, thereby mitigating wear. Prashanth et al. [61] conducted a study on the wear behavior of commercial pure titanium (CP-Ti) components fabricated via SLM and casting techniques. Under scanning electron microscopy (SEM) examination, CP-Ti parts produced through SLM exhibited a martensitic (α') microstructure, whereas the cast samples displayed a plate-like (α) microstructure. Nevertheless, SLM CP-Ti demonstrated superior wear resistance attributed to its martensitic microstructure, finer grain size, and exceptional microhardness. Kang et al. [22] primarily investigated the preparation of polycrystalline aluminum-silicon alloys with ultra-high silicon content using SLM. Their findings revealed that the presence of large primary silicon phases contributes to enhancing the wear resistance of SLM Al-HighSi alloys. Bartolomeu et al. [62,63] explored the influence of processing techniques on the microstructural composition of SLM Ti6Al4V biomedical alloys. Notably, the harder microstructural components present in SLM Ti6Al4V alloys contribute to their superior wear resistance. Additionally, five Ti6Al4V cellular structures with varying pore sizes ranging from 100 to 500 μm were designed and fabricated using SLM. The friction and wear properties of these porous structures were influenced by the pore size, with the structure designed with a 100 μm pore size exhibiting higher wear resistance due to its increased contact area. Zhang et al. [64] discovered that Ti6Al4V composite materials reinforced with Zr-based metallic glass via SLM possess a unique microstructure composed of partially crystallized Zr-based metallic glass (MG) nanoparticles and fine β particles. Micro-scratch tests demonstrated that the hard nano-reinforcement reduces wear volume, offering superior wear resistance compared to unreinforced Ti64 alloy. The DED process was utilized to fabricate WC-12Co cemented carbides, and their wear characteristics were compared with those of WC-12Co coatings produced via the high-velocity oxygen fuel (HVOF) thermal spray technique in [65]. Results showed that DED materials exhibited lower wear rates compared to HVOF materials. The difference in wear behavior between DED and HVOF materials can be attributed to the presence of rough WC particles in DED samples, with DED bulk materials displaying superior wear resistance compared to HVOF coating materials. Madhukar et al. [66] successfully fabricated functionally graded materials (FGM) using the dual-wire arc additive manufacturing with tungsten inert gas (WAAM-TIG) process, which exhibited impeccable dimensional accuracy and was devoid of defects such as cracks and pores. Within continuous gradient (CG-FGM) materials,

an increase in Inconel 625 content led to a corresponding elevation in friction coefficient, whereas the wear rate exhibited a decrease. Conversely, in sandwich structure (SW-FGM) materials, both friction coefficient and wear rate were primarily influenced by the chosen FGM design. Lei et al. [67] conducted a study utilizing gaussian lasers and circular oscillation laser deposition equipment to fabricate NiCu alloy and 16 wt.% WC/NiCu composite materials, respectively. Their findings revealed that materials produced using circular oscillation lasers exhibited finer grain structures, resulting in a 15% and 11.1% enhancement in microhardness, and a significant reduction in wear rates by 76.5% and 22.2%, respectively, compared to those prepared with Gaussian lasers (Figures 2 and 3).

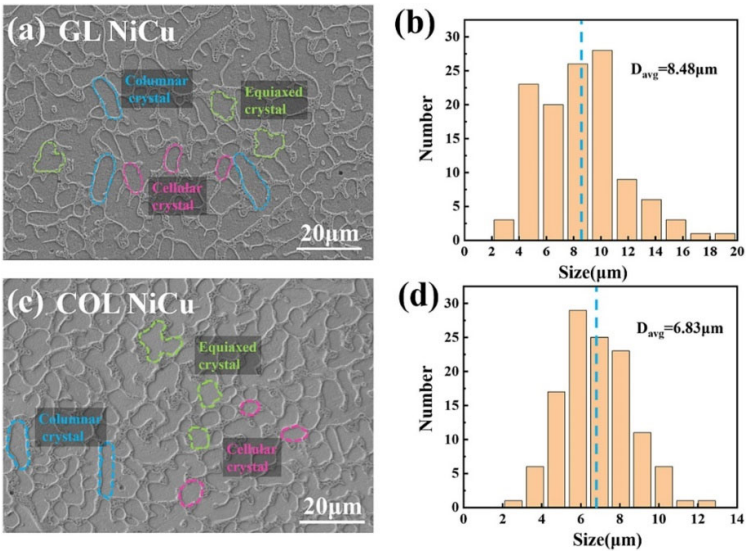

Figure 2. The microstructure of (**a**) GL NiCu and (**c**) COL NiCu. The particle size distribution of (**b**) GL NiCu and (**d**) COL NiCu [67].

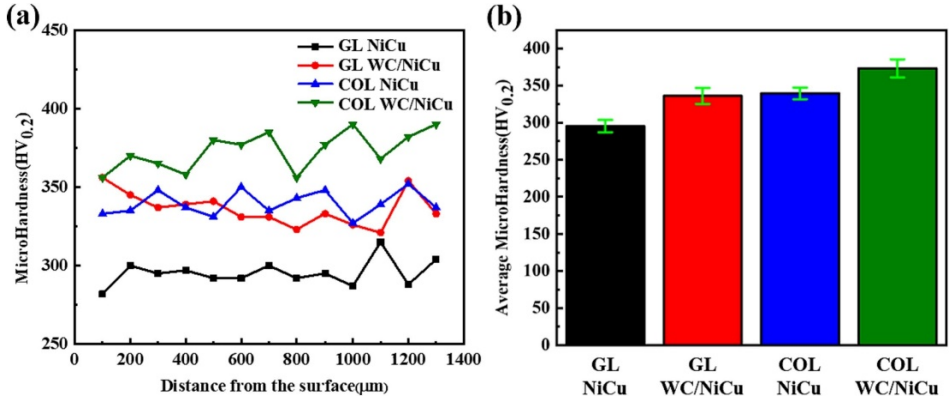

Figure 3. (**a**) Microhardness curves of four materials. (**b**) Average microhardness with standard error [67].

The anisotropy of microstructure significantly impacts the mechanical properties and wear resistance of materials during additive manufacturing processes. Zhu et al. [68] fabricated 316L stainless steel samples utilizing SLM technology, revealing that wear anisotropy is particularly evident under low loads, particularly on the lateral surfaces. This anisotropy arises from the varying sliding resistance of the columnar structure along different sliding directions, resulting in both the highest and lowest wear rates. Under high loads, this difference becomes less significant, and the wear behavior exhibits isotropic characteristics (Figure 4). Krick et al. [69] discovered that variations in construction direction and whisker orientation contribute to the anisotropy observed in the wear properties of AMed epoxy-based nanocomposites. Optimal wear performance was attained by aligning the

whiskers to the opposing surface of the sliding steel and sliding orthogonally to both the construction direction and printing path. In a separate study, Afshari et al. [70] examined the microstructure and tribological characteristics of PH13-8Mo stainless steel fabricated using WAAM under diverse heat treatment conditions. Their findings reveal that the microstructure characteristics and morphological anisotropy of reverse-transformed austenite significantly impact wear performance. Notably, the anisotropy of the microstructure primarily manifests as anisotropic wear resistance during shorter sliding periods of 600 s, whereas periods of 1800 s elicit an isotropic wear response.

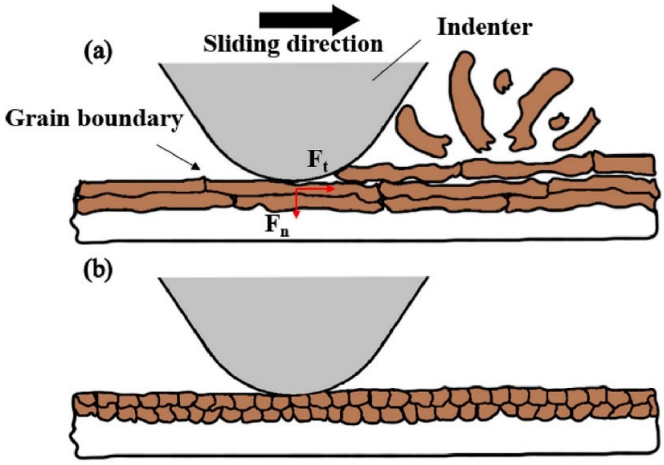

Figure 4. (**a**) The columnar cells are parallel to the sliding direction; (**b**) the columnar cells are perpendicular to the sliding direction [68].

3.3. Wear of Materials for Repair in Additive Manufacturing

Based on the collected literature, AM materials are extensively utilized in repairing damaged components due to their superior wear resistance and minimal wear. These repaired components exhibit enhanced wear performance, thereby extending their operational lifespan and offering numerous other benefits.

In recent years, there has been extensive research on utilizing additive manufacturing materials for repairing components in the automotive and aviation sectors. Yang et al. [32] conducted a study on the application of iron-based, nickel-based, and cobalt-based self-fluxing alloy powders as repair materials in laser cladding layers. Their findings revealed that the wear resistance of wheel steel samples repaired through laser additive manufacturing techniques was significantly enhanced to varying degrees. Zhao et al. [71] explored the feasibility of repairing damaged aircraft engine casings using AlSi10Mg alloy and the LMD process. The results demonstrated that the COF and wear rate of the AlSi10Mg repair layers fabricated through the LMD process were comparable to those of the original aircraft engine shells, thus fulfilling the wear resistance requirements for engine shell repairs. For the restoration of non-uniform high-temperature alloy components in the aviation industry, a hybrid approach combining "laser surface re-melting (LSM) and directional energy deposition" was employed to repair IC10 directionally solidified high-temperature alloy [72]. The results indicated that the repaired alloy substrate exhibited the best wear resistance, whereas the heat-affected zone demonstrated the poorest wear resistance. The wear resistance of the deposited layer fell between these two extremes, gradually decreasing from the bottom to the top. Nickel-based high-temperature alloys possess exceptional high-temperature strength and oxidation resistance, making them widely utilized in critical components such as aircraft engines and turbine blades. However, these components are susceptible to wear and tear, including ablation, fracture, and chipping, due to prolonged exposure to harsh conditions like high temperature and pressure. Fortunately, the application of specialized additive manufacturing repair techniques can effectively restore the dimensions and performance of damaged parts [73]. Chen et al. [74] discovered that single-crystal nickel-based high-temperature alloy samples fabricated through

additive manufacturing techniques exhibit remarkable wear resistance, thereby providing experimental backing for the utilization of laser additive manufacturing in repairing and enhancing the lifespan of the tenon of single-crystal nickel-based high-temperature alloy turbine blade tenons.

Extensive research has used various additive repair techniques across diverse fields. Lewis et al. [75] evaluated the suitability of laser cladding (LC) as a method for repairing or treating new tracks, delving into its wear and rolling contact fatigue (RCF) performance in railway applications. Shanmugam et al. [9] examined the wear behavior of austenitic stainless steel 347 samples fabricated using WAAM at elevated temperatures. Their findings revealed that an increase in the Fe_4O_3 percentage at high temperatures facilitates the repair of worn surfaces through the formation of a mechanically mixed composite layer. Chen et al. [29] focused on laser-based repair of worn and corroded components, discovering that the 30Cr15MoY alloy steel coating produced by laser direct metal deposition (DLMD) technology exhibited the lowest wear rate when the energy per unit volume deposition (EVD) was set to 128 J/mm. Reséndiz-Calderón et al. [76] investigated the impact of boron treatment on the repair of low-carbon steel through arc welding. Their results demonstrated that boron treatment significantly enhances the hardness and wear resistance of the repaired steel. Extensive research has been conducted on laser additive repair technology to address the critical need for edge damage restoration in TC17 titanium alloy components [77]. The findings reveal that the wear resistance of the laser-repaired zone in TC17 titanium alloy surpasses that of the original substrate, with notable improvements ranging from 23% to 69% and peaking at 77% from the top to the bottom of the repaired area. Alidokht et al. [78] employed spherical nickel powder along with two distinct types of WC particles as raw materials to fabricate multimodal Ni-24 vol% WC composite coatings through cold spraying technology, a process that generates thick and dense deposits, ideal for additive manufacturing or the restoration of damaged components. To tackle the challenge of worn camshafts, Chen et al. [51] utilized the pre-set powder laser cladding (PPLC) technique to fabricate T15 alloy steel coatings with varying Cr concentrations. The analysis indicates that an increase in Cr content leads to a decrease in wear resistance. Notably, the T15 alloy steel coating with a chromium content of 10.04% exhibits the highest wear resistance, offering valuable insights for optimizing the composition of high-speed steel to achieve desired wear resistance properties.

Overall, utilizing suitable additive technologies to restore damaged and failed components can effectively enhance their wear resistance. For example, concerning the wheel steel samples repaired using laser additive technology, the Co-based alloy coating exhibited the lowest friction coefficient, approximately 0.41. The friction coefficients for the Fe-based and Ni-based alloy coating samples were 0.63 and 0.75 in [32], respectively. Chen et al. [74] found that the friction coefficient of single-crystal nickel-based high-temperature alloy samples produced via additive manufacturing was reduced by approximately 10% compared to traditionally cast samples. Chen et al. [29] discovered that at a laser energy density of 128 J/mm^3, the 30Cr15MoY alloy steel repair coating demonstrated a wear rate of 6.49 $\times$ 10^{-6} mm^3/(N·mm). Nevertheless, the available research outcomes on the application of additive manufacturing in the realm of repair and maintenance remain limited. Consequently, this review concludes with a tabular compilation of pertinent literature, as presented in Table 3, to facilitate future researchers in exploring this promising field further.

Table 3. Research findings in additive manufacturing repair.

Repair Object	Additive Technology	Research Focus	Reference
Wheel steel	LC	The wear resistance of wheel steel samples after additive repair has been improved to varying degrees	[32]
Aircraft engine casing	LMD	The AlSi10Mg repair layer sample can meet the wear resistance requirements for aircraft engine shell repair	[71]
High-temperature alloy components	LSM + DED	Microstructure and wear behavior of different regions of IC10 directionally cured high-temperature alloy repaired with DED	[72]

Table 3. *Cont.*

Repair Object	Additive Technology	Research Focus	Reference
Single-crystal nickel-based high-temperature alloy turbine blade tenon	LAM	Application of LAM in repairing and extending the service life of single-crystal nickel-based high-temperature alloy turbine blade tenons	[74]
Railway	LC	Analyzing the wear and rolling contact fatigue (RCF) performance of LC process in railway applications	[75]
Easy-to-wear parts	WAAM	Study on the tribological properties of austenitic stainless steel 347 specimens prepared by WAAM under high-temperature and non-lubricated conditions	[9]
Failed components	DLMD	Study on the effect of EVD on the wear resistance and corrosion resistance of DLMDed 30Cr15MoY alloy steel coating for laser repair of worn and corroded components	[29]
Mild steel	WAAM	Borination treatment can effectively improve the hardness and wear resistance of repaired low-carbon steel	[76]
TC17 titanium alloy components	LAM	Research on laser additive repair process for edge damage repair of TC17 titanium alloy components	[77]
Damaged components	Cold spray technology	The research proves that the cold spray produces thick and dense deposits, which can be used to manufacture additives or repair damaged parts	[78]
Camshaft	PPLC	A guideline for high-speed steel with ideal wear resistance is provided for repairing worn camshafts	[51]

4. Wear in Additive Manufacturing Processes

4.1. The Influence of Process Parameters on Wear

During the preparation process of various additive manufacturing techniques, numerous process parameter settings are involved. The variance in these parameters leads to distinct wear properties in the fabricated components and materials. Consequently, proactive control of process parameters is crucial for minimizing wear and damage in additive manufacturing parts.

According to the comprehensive literature review, various process parameters involved in SLM technology govern the mechanical and wear behavior of parts. Numerous studies have focused on altering the process parameters of SLM additive technology to fabricate materials, ultimately aiming to enhance their wear performance. Zhu et al. [79] tailored the microstructure of 316L stainless steel produced via SLM technology by employing three distinct scanning strategies. Their findings revealed that the serrated R90 sample exhibited the most significant improvement in wear resistance, with a remarkable reduction in scratch depth and wear rate by 90.8% and 96.7%, respectively. Huang et al. [80] examined the impact of varying energy densities on the porosity of 316L stainless steel, which subsequently influenced the density of the samples and their micro-motion wear characteristics. Their investigation revealed that within a specific range of energy densities, a decrease in energy density led to a corresponding decrease in material density and a deterioration in wear resistance. Apart from studies on 316L stainless steel, research has also been conducted on aluminum-silicon alloys and Inconel 718 composite materials. The wear rate of the SLM ultra-crystalline aluminum-silicon alloy with ultra-high silicon content is minimized at a laser power of 350 W, approximately 5.5×10^{-4} $mm^3/(N \cdot m)$, surpassing the wear rate of the SLM Al-18Si alloy [22]. Rong et al. [81] conducted a study on the influence of laser energy line density (η) and laser scanning speed on the performance of tungsten carbide (WC_{1-x})-particle-reinforced SLM Inconel 718 composite components. Their findings revealed that, at an optimal η of 242 J/m, the microhardness peaked at 389.4 $HV_{0.1}$ (Vickers hardness, i.e., an indicator of Vickers hardness, representing the hardness value measured under a load of 0.1 kilogram-force), accompanied by a friction coefficient of 0.39 and a wear rate of 2.3×10^{-4} $mm^3/(N \cdot m)$. In another study, when the optimal scanning speed was set to 450 mm/s, the SLM WC/Inconel 718 composite exhibited a gradient interface, resulting in a friction coefficient of 0.35 and a wear rate of 2.5×10^{-4} $mm^3/(N \cdot m)$ [16]. Notably, the study underscores the significance of the gradient interface created by varying the laser scanning speed in enhancing the wear performance of the composite material. Additionally, the collected literature also encompasses research on various other SLM materials. Specifically, regarding titanium-related materials, the combined influence of SLM scanning speed and laser energy density has been observed to induce micro-ball pressing phenomena

and interlayer thermal microcracks, ultimately affecting their wear performance [82,83]. Kang et al. [84] successfully fabricated TiB-reinforced titanium matrix composites through the selective laser melting of a blend of CrB_2 and commercially pure titanium powder. Their research revealed that materials processed at both high and low scanning speeds exhibit superior hardness and reduced wear rates compared to those processed at medium scanning speeds while maintaining the highest density. Dong et al. [85] conducted a comprehensive study on the anisotropic wear resistance of CoCrW alloys fabricated via SLM at varying scanning speeds. Notably, the wear rate of the SLM CoCrW alloy was observed to be higher on the FD-SD plane compared to the BD-SD plane. Interestingly, the friction coefficient on the BD-SD plane remained relatively consistent, approximately 0.60, across different laser scanning rates. Guo et al. [86] employed the SLM technique to produce NiTi alloys and systematically explored the influence of scanning speed and laser power on their wear properties. Remarkably, the absence of cracks and minimal porosity in the SLM-processed NiTi alloys under various parameters contributed to their exceptional wear resistance. Liu et al. [30] delved into the impact of scanning speed, ranging from 600 to 800 mm/s, on the microstructure, microhardness, and friction-corrosion behavior of SLM Fe-Mn alloys. Their findings revealed that samples processed at a scanning speed of 700 mm/s exhibited the lowest corrosion wear rate.

Powder bed fusion (PBF) is an additive manufacturing technique utilized for fabricating components, with its processing parameters serving as the cornerstone for determining the wear rate of these components. Numerous studies have delved into the intricate relationship between the process parameters and wear friction characteristics of PBF technology. The meticulous selection of PBF processing parameters is paramount for minimizing wear rates, as parts with optimal compaction typically exhibit superior wear resistance. By leveraging diverse wear mechanisms and laser sintering methodologies, along with proactive modulation of PBF process parameters and powder composition, the wear resistance of components can be significantly enhanced [87]. Wu et al. [88] employed X-ray diffraction to identify the phases present in AlMgScZrMn alloys fabricated via L-PBF technology, with volumetric energy densities ranging from 52 to 102 J/mm^3. They evaluated the wear properties of these alloys against SiC balls, the findings reveal that samples produced with a volume energy density of 67 J/mm^3 exhibit superior hardness and finer grain structure, thereby enhancing the wear resistance of the AlMgScZrMn alloy. Furthermore, He et al. [89] successfully fabricated crack-free pure molybdenum with a relative density of 99.2% using the L-PBF process, employing a layer thickness of 30 μm and a high power setting of 350 W. Notably, the wear rate of the AMed Mo was observed to be higher compared to traditionally manufactured samples.

Regarding the investigation of process parameters of alternative additive technologies on additive manufacturing wear, Bordin et al. [90] conducted an assessment of the tool wear mechanisms encountered during semi-precision machining of electron-beam-melted (EBM) Ti6Al4V, utilizing WC coatings under both dry and low-temperature conditions across varying cutting speeds and feed rates. The findings revealed that an increase in both cutting speed and feed rate led to a corresponding elevation in tool wear. However, interestingly, when compared to dry cutting, the application of low-temperature cooling was observed to mitigate the adhesive wear mechanism occurring on the tool's cutting surface due to the workpiece material, thereby demonstrating the viability of utilizing low-temperature cooling to mitigate tool wear during the processing of EBMed Ti6Al4V. Kurzynowski et al. [91] designed a laser surface alloying (LSA) technique utilizing rhenium, adjusting the laser power and powder feed rate parameters to fabricate Re powder layers with fully dissolved 718—14% Re layers and partially dissolved 718—28% Re layers on Inconel 718 alloy. When compared to the Inconel 718 substrate, alloying with 28 wt.% rhenium significantly enhanced the wear resistance of the Inconel 718 substrate, resulting in a reduction of 82% in its sliding wear rate and a 25% increase in its wear resistance index. Gong et al. [23] utilized laser additive manufacturing (LAM) technology to fabricate Inconel 718 high-temperature alloy at varying laser powers. Dry sliding tests were conducted, and

the worn surfaces were subsequently analyzed using laser scanning confocal microscopy (LSCM) and scanning electron microscopy (SEM). The findings revealed that at an optimal laser power of 1200 W, a relatively stable friction state was achieved, accompanied by the lowest wear rate of 1.355 × 10^{-3} mm^3/(N·m) during the wear process. Chen et al. [29] explored the impact of laser energy volume density (EVD) on the wear and corrosion resistance of 30Cr15MoY alloy steel coatings fabricated through laser direct metal deposition (DLMD). Their results demonstrated that the sample with an EVD of 128 J/mm exhibited the highest hardness and lowest wear rate. Beheshti et al. [92] investigated the tribological behavior of Inconel 625 samples produced using PBF technology, considering varying layer thicknesses and printing orientations. Their results included thinner layer defects and superior surface finish, leading to finer microstructures, enhanced oxidation rates, improved friction layers, and ultimately reduced wear. Yao [93] and others discovered that LC process parameters significantly influence the macroscopic morphology and microstructure of LC-HEACs. Appropriate selection of process parameters can markedly enhance the wear resistance of coatings. During the L-DEDed process for titanium-based composite materials, equiaxed and dendritic TiC morphologies were achieved by adjusting the laser scanning speed and power [21]. The shift in TiC morphology in the sample triggered a change in the wear mechanism, leading to a reduction in wear resistance. Compared to samples with equiaxed TiC, the wear resistance improved by 59%. Lin et al. [94] and others modified the laser scanning rate while laser-adding Ni-Cr-Cu onto the surface of Q235 carbon steel. The findings revealed that, across the tested laser parameters, the cladding layer produced at the higher scanning rate (700 mm/min) exhibited optimal hardness and wear resistance.

In summary, the process parameters in various additive manufacturing techniques, including energy density, scanning speed, and laser power, exert a significant influence on the wear resistance of materials. Optimizing these parameters not only enhances the mechanical properties of materials but also boosts the reliability and durability of the final products. For instance, Zhu et al. [79] reported a 90.8% reduction in scratch depth and a 96.7% decrease in wear rate for additive manufacturing samples employing various scanning strategies, while Rong et al. [81] demonstrated enhanced wear performance under optimal η conditions, achieving a hardness of 389.4 $HV_{0.1}$, a friction coefficient of 0.39, and a wear rate of 2.3 × 10^{-4} mm^3/(N·m). Kang et al. [84] evaluated the wear performance of samples at high, medium, and low scanning speeds, revealing that those scanned at high and low speeds exhibited greater hardness and lower wear rates compared to those scanned at moderate speeds.

In this review, the collected literature is summarized, as presented in Table 4. Future research should focus on identifying the optimal combinations of process parameters with various materials and manufacturing techniques to enhance wear resistance and improve performance. With a deeper understanding of these influencing factors, the additive manufacturing industry can better fulfill the requirements of high-performance applications, particularly in cutting-edge sectors such as the aerospace, automotive, and biomedicine sectors.

Table 4. Discovery of the influence of additive technology process parameters on wear.

Additive Technology	Additive Objects	Process Parameters	Research Findings	Reference
SLM	316l stainless steel	Scanning strategy	The zigzag-R90 sample showed the greatest enhancement in wear resistance, with a reduction of 90.8% in scratch depth and 96.7% in wear rate	[79]
SLM	316l stainless steel	Energy density	The lower the energy density, the higher the porosity, the lower the density, and the poorer the wear resistance	[80]
SLM	Supercrystalline aluminum-silicon alloy	Laser power	The wear rate of the sample obtained at a laser power of 350W is the lowest, approximately 5.5 × 10^{-4} mm^3/(N·m)	[22]
SLM	Inconel 718	Laser energy linear density(η)	When the optimal η is 242 J/m, the hardness is 389.4 $HV_{0.1}$, the friction coefficient is 0.39, and the wear rate is 2.3 × 10^4 mm^3/(N·m)	[81]

Table 4. *Cont.*

Additive Technology	Additive Objects	Process Parameters	Research Findings	Reference
SLM	WC/Inconel 718 composite material	Laser scanning rate	Changing the gradient interface generated by laser scanning speed can improve the wear performance of SLM WC/Inconel 718 composite parts	[16]
SLM	Materials related to titanium	Laser energy density	The combined effect of SLM scanning speed and laser energy density leads to the micro-ball pressing phenomenon and the formation of interlayer thermal microcracks in the material, which affects the wear performance	[82,83]
SLM	Near α Ti-matrix composite	Laser scanning rate	The parts obtained at high and low scanning speeds have higher hardness and lower wear rate than those obtained at medium scanning speeds, with the highest density	[84]
SLM	CoCrW alloy	Laser scanning rate	The anisotropic wear resistance of CoCrW alloy prepared by SLM. The wear rate of SLM CoCrW alloy FD-SD plane is higher than that of the BD-SD plane	[85]
SLM	NiTi alloy	Laser scanning rate Laser power	The SLM NiTi alloy obtained under different parameters exhibits excellent wear resistance, no cracks, and low porosity	[86]
SLM	Fe-Mn alloy	Laser scanning rate	The sample processed at a scanning speed of 700 mm/s has the lowest wear rate	[30]
PBF	PBF materials	Machining parameter	Actively control PBF process parameters and powder composition to improve the wear resistance of parts	[87]
L-PBF	AlMgScZrMn alloy	Volumetric energy density	The sample prepared with 67 J/mm^3 has the best wear resistance performance	[88]
L-PBF	Pure molybdenum	Powder layer thickness power	The wear rate of Mo in additive manufacturing is higher	[89]
EBM	Ti6Al4V	Cutting rate, feed rate, low-temperature cooling	The higher the cutting speed and feed rate, the higher the tool wear. Compared with dry cutting, low-temperature cooling can reduce the wear of the workpiece on the cutting surface of the tool	[90]
LSA	Inconel 718 alloy	Laser power powder feed rate	Alloying with 28 wt.% rhenium improved the wear resistance of Inconel 718 substrate, reducing its sliding wear rate by 82% and increasing its wear resistance index by 25%	[91]
LAM	Inconel 718 high-temperature alloy	Laser power	At the optimal laser power of 1200W, a relatively stable friction state and a minimum wear rate of 1.355×10^{-3} mm^3/(N·m) were achieved	[23]
DLMD	30Cr15MoY alloy steel	Energy volume density	Sample with an EVD of 128 J/mm has the highest hardness and lowest wear rate	[29]
PBF	Inconel 625	Layer thickness print orientation	Studied the friction and wear behavior of Inconel 625 samples prepared by PBF technology with different layer thicknesses and printing orientations	[92]
LC	High-entropy alloys	Laser power scanning rate and laser spot size	Reasonably selecting appropriate process parameters can significantly improve the wear resistance of coatings	[93]
L-DED	Titanium matrix composites	Scanning speed, laser power	The transformation of TiC morphology leads to a change in wear mechanism and alters wear resistance	[21]
LAM	Q235 carbon steel	Laser scanning rate	The hardness and wear resistance of the cladding layer generated at a scanning rate of 700 mm/min is the best	[94]

4.2. The Effect of Heat Treatment on Wear

Heat treatment is a technique used to modify the microstructure and properties of materials through controlled heating and cooling processes. It applies to a variety of materials including metals, ceramics, and polymers. A composite coating was fabricated on a Ti6Al4V alloy substrate via laser cladding, and the study examined the impact of heat treatment on the coating's microstructure, microhardness, and fracture toughness [95]. The findings revealed that specific heat treatment (heating to 500 °C for 1 h) notably reduces both the magnitude and variability of the friction coefficient while having minimal influence on wear mass and volume loss. Lorusso et al. [96] found that metal alloys produced via L-PBF exhibit greater wear resistance under dry and boundary lubrication conditions compared to those created using traditional methods. Typically, heat treatment diminishes wear resistance and elevates the COF. Heat treatment was applied to Inconel 718 samples produced using SLM at various temperatures to assess its influence on the samples' microstructure, microhardness, and wear behavior [97]. Research indicates that heat treatment temperatures can modify the microstructure of samples, and specimens

fabricated via SLM demonstrate enhanced wear resistance post-heat treatment at specific temperatures, surpassing samples produced using conventional methods. Kaynak et al. [98] investigated the effects of various heat treatment temperatures on SLM 316L stainless steel samples, examining their microstructure, microhardness, XRD response, porosity, and wear behavior. The findings reveal that heat treatment temperatures significantly influence the evolution of microstructure, XRD response, and porosity of the samples. Haden et al. [99] developed TiC-reinforced H13 steel matrix composites using laser deposition technology and assessed the impact of tempering on the composites' microstructure and performance. The study revealed that as TiC content increases, both the hardness and wear resistance of the composite improve. Although the hardness of tempered samples is lower than that of their untempered counterparts, their wear resistance is heightened. Podgornik et al. [100] explored the impact of build orientation and heat treatment on the wear resistance of martensitic age-hardened steel produced via laser powder bed fusion (L-PBF). Wear-related studies noted that age-hardening heat treatments enhance the uniformity of the microstructure in additively manufactured martensitic steel, thereby influencing its wear resistance. Hemachandra et al. [58] reviewed the microstructures and tribological behaviors of three distinct alloy systems in additive manufacturing: aluminum, titanium, and steel. The study found that the influence of heat treatment on the wear behavior of AM components varies with the type and composition of the material. Within the Al-Si alloy system, heat treatment disrupts the Si network into a delicate porous structure and induces Si precipitates within the aluminum matrix, leading to a decrease in wear resistance. Heat treatment of 316L stainless steel results in the roughening of the grain structure and the closing of porosity, thereby enhancing its wear resistance post-treatment. Additionally, heat treatment of SLM Ti64 samples moderately affects their wear resistance. Chen et al. [101] subjected laser-additively manufactured AISIH13 tool steel to heat treatments at 350, 450, 550, 600, and 650 °C for 2 h each. The research revealed that tempering transforms martensite into tempered martensite and precipitates fine alloy carbides within the matrix. Samples tempered at 550 °C exhibit a greater wear volume loss than those tempered at between 600 and 650 °C. Afshari et al. [70] investigated PH13-8Mo stainless steel produced via metal wire arc additive manufacturing, under various heat treatment conditions. The findings revealed that all heat treatment cycles enhanced the wear resistance of WAAM PH13-8Mo at 1800 s, with the specimen heat-treated at 500 °C exhibiting superior wear performance. A comparative analysis of material properties for Inconel 718 parts fabricated using the L-PBF method, before and after heat treatment, showed a slight reduction in porosity. Heat treatment altered the internal grain structure and microstructure of the parts, leading to a 10% increase in microhardness and a 14% improvement in wear resistance [102]. Lopes et al. [103] conducted an in-depth study on various heat treatments to understand the evolution of microstructure, examining the mechanical strength, fracture toughness, and wear resistance of H13 tool steel processed with L-PBF. The results showed that low-temperature tempering at 550 °C yielded the lowest wear rate, approximately $2.0 \times 10^{-5} mm^3/(N \cdot m)$. Conversely, high-temperature tempering at 650 °C, combined with prior austenitization and quenching, resulted in a wear rate of $3.4 \times 10^{-5} mm^3/(N \cdot m)$. Consequently, the selection of heat treatment processes can be tailored to meet specific project requirements.

In summary, heat treatment significantly influences the wear performance of materials produced via additive manufacturing, aiding researchers in developing materials with superior friction and wear characteristics. For instance, in [97], heat treatment was applied to SLM Inconel 718 samples, altering their microstructure and enhancing their wear resistance relative to conventionally manufactured samples. Podgornik et al. [100] indicated that heat treatment enhances the microstructural uniformity of martensitic age-hardened steel produced via additive manufacturing, thereby influencing its wear resistance. Building on this, this section primarily explores the effects of heat treatment on wear issues in additive manufacturing, offering a theoretical framework for future research in this field.

5. Conclusions and Future Directions

5.1. Conclusions

In summary, recent advancements have spurred the emergence of numerous new AM technologies and materials, significantly advancing the mitigation of wear issues in the additive manufacturing process. The reviewed literature categorizes and discusses the wear issues encountered in additive manufacturing processes. The following insights emerge from this review:

- Through an in-depth analysis of the wear mechanisms in components produced via additive manufacturing and an examination of how different types of wear affect their performance, it is evident that given various additive manufacturing techniques, understanding the wear mechanisms allows us to identify the primary types of wear. Subsequently, appropriate measures can be taken to minimize wear.
- The composition of materials used in additive manufacturing is modified by incorporating new elements or adjusting their concentrations. Composite materials, created using suitable additive manufacturing techniques, exhibit significant improvements in wear resistance. The available literature predominantly focuses on the incorporation of TiC and WC.
- A material's microstructure is one of the key factors determining its wear performance, and changes in microstructure can affect the mechanical properties, thereby influencing its wear performance. Most of the literature reviewed in this article focuses on the microstructure of alloys, with less attention to other materials. As research progresses, we have seen the emergence of more innovative and sophisticated alloys and manufacturing techniques. This is particularly evident in the realm of how additive manufacturing influences and generates microstructures and how these microstructures impact wear resistance.
- Additive repair applied to important components in industrial sectors such as vehicles and aviation is also a research hotspot. For high-temperature alloy components in aviation, additive technology can be used for repairs to enhance wear resistance. Research has also been conducted on optimizing the repair of high-speed steel, resulting in some additive repair materials with significant wear-related advantages.
- Changing the process parameters in additive manufacturing technology can influence the material's microstructure and reduce porosity and defects, thereby affecting the wear performance of materials or components, including wear rate, wear resistance, and wear volume.
- The application of different heat treatment processes to materials produced via various additive manufacturing techniques can differentially impact their wear performance.

5.2. Future Directions

In the field of additive manufacturing, enhancing wear performance is a crucial area of research. As industry demands for the performance of additively manufactured components continue to rise, future research will concentrate on key areas to improve the wear resistance of these parts. Below are some potential future research directions:

- Exploration and development of new materials: Researchers should concentrate on developing novel alloys or composite materials to enhance the wear resistance of additively manufactured components.
- Optimizing microstructure: By researching laser processes and powder handling in additive manufacturing, optimizing the microstructure of manufactured components (e.g., morphology, phase composition, and grain orientation) can significantly enhance their hardness and wear resistance.
- The significance of additive manufacturing in the repair sector cannot be overlooked. As additive manufacturing technology continues to advance and expand its applications, its potential in the repair industry will become even more pronounced in the future.
- Investigating various post-processing techniques, such as heat treatment and surface hardening, to assess their impact on the wear resistance of additively manufactured

components. These techniques can enhance material hardness and wear resistance, thereby prolonging the lifespan of components.

Author Contributions: Conceptualization, X.J.; methodology, X.J. and J.L.; validation, X.J.; formal analysis, N.Z.; investigation, X.J., J.L., N.Z. and Z.Z.; writing—original draft preparation, J.L.; writing—review and editing, Z.C. and Z.Z.; visualization, N.Z.; supervision, X.J.; project administration, Z.C.; funding acquisition, X.J. and Z.Z. All authors have read and agreed to the published version of the manuscript.

Funding: This research was funded by the Natural Science Basic Research Program of Shaanxi Province grant number 2023-JC-ZD-29, 2023-GHZD-35, and 2024JC-ZDXM-25 and the Key Research and Development Program of Shaanxi grant number 2024GX-YBXM-208.

Data Availability Statement: No new data were created or analyzed in this study. Data sharing is not applicable to this article.

Conflicts of Interest: Author N.Z. is employee of China International Engineering Consulting Corporation. Other authors declare no conflict of interest.

References

1. Ngo, T.D.; Kashani, A.; Imbalzano, G.; Nguyen, K.T.Q.; Hui, D. Additive manufacturing (3D printing): A review of materials, methods, applications and challenges. *Compos. Part B* **2018**, *143*, 172. [CrossRef]
2. Massola, C.P.; Chaves, A.P.; Albertin, E. A discussion on the measurement of grinding media wear. *J. Mater. Res. Technol.* **2016**, *5*, 282. [CrossRef]
3. Renner, P.; Jha, S.; Chen, Y.; Raut, A.; Mehta, S.G.; Liang, H. A Review on Corrosion and Wear of Additively Manufactured Alloys. *J. Tribol.* **2021**, *143*, 050802. [CrossRef]
4. Orgeldinger, C.; Seynstahl, A.; Rosnitschek, T.; Tremmel, S. Surface Properties and Tribological Behavior of Additively Manufactured Components: A Systematic Review. *Lubricants* **2023**, *11*, 257. [CrossRef]
5. Zhu, Y.; Chen, X.; Zou, J.; Yang, H. Sliding wear of selective laser melting processed Ti6Al4V under boundary lubrication conditions. *Wear* **2016**, *368*, 485–495. [CrossRef]
6. Kang, N.; El Mansori, M. A new insight on induced-tribological behaviour of hypereutectic Al-Si alloys manufactured by selective laser melting. *Tribol. Int.* **2020**, *149*, 105751. [CrossRef]
7. Huttunen-Saarivirta, E.; Heino, V.; Vaajoki, A.; Hakala, T.J.; Ronkainen, H. Wear of additively manufactured tool steel in contact with aluminium alloy. *Wear* **2019**, *432*, 202934. [CrossRef]
8. Aziz, R.; Ul Haq, M.I.; Raina, A. Effect of surface texturing on friction behaviour of 3D printed polylactic acid (PLA). *Polym. Test.* **2020**, *85*, 106434. [CrossRef]
9. Duraisamy, R.; Kumar, S.M.; Kannan, A.R.; Shanmugam, N.S.; Sankaranarayanasamy, K.; Ramesh, M.R. Tribological performance of wire arc additive manufactured 347 austenitic stainless steel under unlubricated conditions at elevated temperatures. *J. Manuf. Process.* **2020**, *56*, 306–321. [CrossRef]
10. Parvaresh, B.; Salehan, R.; Miresmaeili, R. Investigating Isotropy of Mechanical and Wear Properties in As-Deposited and Inter-Layer Cold Worked Specimens Manufactured by Wire Arc Additive Manufacturing. *Met. Mater. Int.* **2020**, *27*, 92–105. [CrossRef]
11. Ferreira, D.F.S.; Vieira, J.S.; Rodrigues, S.P.; Miranda, G.; Oliveira, F.J.; Oliveira, J.M. Dry sliding wear and mechanical behaviour of selective laser melting processed 18Ni300 and H13 steels for moulds. *Wear* **2022**, *488*, 204179. [CrossRef]
12. Gain, A.K.; Zhang, L. Tribological behavior of eutectic Al–12Si alloy manufactured by selective laser melting. *Wear* **2023**, *522*, 204679. [CrossRef]
13. Herrera, P.; Hernandez-Nava, E.; Thornton, R.; Slatter, T. Abrasive wear resistance of Ti-6AL-4V obtained by the conventional manufacturing process and by electron beam melting (EBM). *Wear* **2023**, *524*, 204879. [CrossRef]
14. Yadav, A.; Srivastava, M.; Jain, P.K.; Rathee, S. Microstructure transformations and improving wear resistance of austenitic stainless steel additively fabricated by arc-based DED process. *Def. Technol.* **2024**, *38*, 194–204. [CrossRef]
15. Yadav, A.; Srivastava, M.; Jain, P.K.; Rathee, S. Microstructure and tribological behaviour of dissimilar steel functional structure developed via arc-based DED process. *Tribol. Int.* **2024**, *197*, 109782. [CrossRef]
16. Rong, T.; Gu, D.; Shi, Q.; Cao, S.; Xia, M. Effects of tailored gradient interface on wear properties of WC/Inconel 718 composites using selective laser melting. *Surf. Coat. Technol.* **2016**, *307*, 418. [CrossRef]
17. Tocci, M.; Pola, A.; Girelli, L.; Lollio, F.; Montesano, L.; Gelfi, M. Wear and Cavitation Erosion Resistance of an AlMgSc Alloy Produced by DMLS. *Metals* **2019**, *9*, 308. [CrossRef]
18. Kc, S.; Nezhadfar, P.D.; Phillips, C.; Kennedy, M.S.; Shamsaei, N.; Jackson, R.L. Tribological behavior of 17–4 PH stainless steel fabricated by traditional manufacturing and laser-based additive manufacturing methods. *Wear* **2019**, *440*, 203100. [CrossRef]
19. Li, N.; Wang, Q.; Niu, W.; Han, P.; Guo, N.; Li, S. Microstructure and wear behaviors of 17-4 PH stainless steel fabricated by laser cladding with post laser shock peening treatment. *Wear* **2024**, *538*, 205207. [CrossRef]

20. Liu, J.; Li, C.; Dong, S.; Wang, D.; Chen, Z.; Yan, S.; Liu, X.; Jin, X.; Xu, B. Frictional behavior of selective laser melted brake discs under high-speed braking. *Tribol. Int.* **2024**, *194*, 109474. [CrossRef]
21. Zheng, Y.; Yan, X.; Qiao, G.; Tang, Y.; Geng, Y.; Shao, Z.; Bai, Q. Enhanced wear resistance of TiC/Ti6Al4V composites through changing TiC morphologies in laser direct energy deposition. *Addit. Manuf.* **2024**, *84*, 104134. [CrossRef]
22. Kang, N.; Coddet, P.; Chen, C.; Wang, Y.; Liao, H.; Coddet, C. Microstructure and wear behavior of in-situ hypereutectic Al–high Si alloys produced by selective laser melting. *Mater. Des.* **2016**, *99*, 120–126. [CrossRef]
23. Xu, Y.; Gong, Y.; Li, P.; Yang, Y.; Qi, Y. The effect of laser power on the microstructure and wear performance of IN718 superalloy fabricated by laser additive manufacturing. *Int. J. Adv. Manuf. Technol.* **2020**, *108*, 2245–2254. [CrossRef]
24. Zhao, P.; Li, J.; Zhang, Y.; Li, X.; Xia, M.M.; Yuan, B.G. Wear and high-temperature oxidation resistances of AlNbTaZrx high-entropy alloys coatings fabricated on Ti6Al4V by laser cladding. *J. Alloys Compd.* **2021**, *862*, 158405. [CrossRef]
25. Dangnan, F.; Espejo, C.; Liskiewicz, T.; Gester, M.; Neville, A. Friction and wear of additive manufactured polymers in dry contact. *J. Manuf. Process.* **2020**, *59*, 238–247. [CrossRef]
26. Ramadas, H.; Sarkar, S.; Nath, A.K. Three-body dry abrasive wear properties of 15–5 precipitation hardening stainless steel produced by laser powder bed fusion process. *Wear* **2021**, *470*, 203623. [CrossRef]
27. Vikhareva, A.; Macêdo, G.; Pelcastre, L.; Hardell, J. High temperature tribological behaviour of additively manufactured tool material for applications in press hardening. *Wear* **2021**, *477*, 203859. [CrossRef]
28. Kan, W.H.; Huang, S.; Man, Z.; Yang, L.; Huang, A.; Chang, L.; Nadot, Y.; Cairney, J.M.; Proust, G. Effect of T6 treatment on additively-manufactured AlSi10Mg sliding against ceramic and steel. *Wear* **2021**, *482*, 203961. [CrossRef]
29. Shang, F.; Chen, S.; Zhou, L.; Jia, W.; Cui, T.; Liang, J.; Liu, C.; Wang, M. Effect of laser energy volume density on wear resistance and corrosion resistance of 30Cr15MoY alloy steel coating prepared by laser direct metal deposition. *Surf. Coat. Technol.* **2021**, *421*, 127382. [CrossRef]
30. Liu, P.; Li, G.; Liu, B.; Liao, C.; Baker, I.; Wu, H. Tribocorrosion behavior of additively-manufactured Fe-Mn alloys. *Mater. Lett.* **2023**, *337*, 133949. [CrossRef]
31. Günen, A.; Gürol, U.; Koçak, M.; Çam, G. Investigation into the influence of boronizing on the wear behavior of additively manufactured Inconel 625 alloy at elevated temperature. *Prog. Addit. Manuf.* **2023**, *8*, 1281–1301. [CrossRef]
32. Xiao, Q.; Li, S.; Yang, W.; Yang, C.; Chen, D.; Ding, H.; Wang, W. High-temperature tribological properties of coatings repaired by laser additive manufacturing on railway wheel tread damage. *Wear* **2023**, *520*, 204674. [CrossRef]
33. Teng, J.Z.; Jiang, P.F.; Cong, Q.; Cui, X.H.; Nie, M.H.; Li, X.R.; Zhang, Z.H. A comparison on microstructure features, compression property and wear performance of TC4 and TC11 alloys fabricated by multi-wire arc additive manufacturing. *J. Mater. Res. Technol.* **2024**, *29*, 2175–2187. [CrossRef]
34. Vishnu, V.; Prabhu, T.R.; Imam, M.; Vineesh, K.P. High-temperature dry sliding wear behavior of additively manufactured austenitic stainless steel (316L). *Wear* **2024**, *540*, 205259. [CrossRef]
35. García-Hernández, C.; Naranjo, J.A.; Castro-Sastre, M.Á.; Berges, C.; Fernandez-Abia, A.I.; Martín-Pedrosa, F.; Herranz, G.; García-Cabezón, C. Enhancing wear performance: A comparative study of traditional vs. additive manufacturing techniques for 17–4pH SS. *Wear* **2024**, *540*, 205258. [CrossRef]
36. Chen, D.; Cui, X.; Guan, Y.; Li, X.; Ma, S.; Dai, Z.; Song, Z.; Feng, L.; Jin, G.; Liu, J. Study on enhanced wear resistance of $FeCoCrNi_2MoSi$ high entropy alloy coatings induced by nano-layered eutectic and Laves phase. *Tribol. Int.* **2024**, *194*, 109534. [CrossRef]
37. Zhang, Y.; Liu, Z.; Lv, Z.; Cao, J.; Tong, Y.; Sun, M.; Cui, C.; Wang, X. Effect of SiC and TiC content on microstructure and wear behavior of Ni-based composite coating manufactured by laser cladding on Ti–6Al–4V. *Wear* **2024**, *552*, 205431. [CrossRef]
38. Zhou, Y.; Duan, L.; Wen, S.; Wei, Q.; Shi, Y. Enhanced micro-hardness and wear resistance of Al-15Si/TiC fabricated by selective laser melting. *Compos. Commun.* **2018**, *10*, 64–67. [CrossRef]
39. Zhe, Q.; Yu, C.; Deng, C.; Hu, X.; Yan, X.; Hu, Y.; Liu, M. Effect of TiC on Microstructure and Wear Properties of Inconel 625 Alloy Fabricated via Selective Laser Melting Technology. *China Surf. Eng.* **2021**, *34*, 76–84.
40. Zhu, C.; Fordyce, I.; Sun, S.D.; Annasamy, M.; Fabijanic, D.; Short, K.; Paradowska, A.; Leary, M.; Brandt, M.; Easton, M. Effect of Ti and TiC additions on the microstructure and wear resistance of high chromium white irons produced by laser directed energy deposition. *Wear* **2022**, *510*, 204519. [CrossRef]
41. Hu, J.; Lin, X.; Hu, Y. High wear resistance and strength of Hastelloy X reinforced with TiC fabricated by laser powder bed fusion additive manufacturing. *Appl. Surf. Sci.* **2024**, *648*, 159004. [CrossRef]
42. Li, W.; Yang, X.; Xiao, J.; Hou, Q. Effect of WC mass fraction on the microstructure and friction properties of WC/Ni60 laser cladding layer of brake discs. *Ceram. Int.* **2021**, *47*, 28754–28763. [CrossRef]
43. Yi, J.L.; Liao, H.L.; Chang, C.; Yan, X.C.; Liu, M.; Zhou, K.S. Reinforcing effects of nano-WC in AlSi10Mg alloy assisted by in-situ surface modification approach. *Trans. Nonferrous Met. Soc. China* **2024**, *34*, 50–64. [CrossRef]
44. Rose, D.; Wolfe, T.; Henein, H. Microstructural Characterization and Wear Resistance of 60 wt.%, 70 wt.%, and 80 wt.% WC-NiCrBSi Thin Walls Deposited Using Plasma Transferred Arc Additive Manufacturing. *JOM* **2023**, *76*, 42. [CrossRef]
45. Patil, A.S.; Hiwarkar, V.D.; Verma, P.K.; Khatirkar, R.K. Effect of TiB2 addition on the microstructure and wear resistance of Ti-6Al-4V alloy fabricated through direct metal laser sintering (DMLS). *J. Alloys Compd.* **2019**, *777*, 165–173. [CrossRef]
46. Wang, H.; Chen, T.; Cong, W.; Liu, D. Laser Cladding of Ti-Based Ceramic Coatings on Ti6Al4V Alloy: Effects of CeO_2 Nanoparticles Additive on Wear Performance. *Coatings* **2019**, *9*, 109. [CrossRef]

47. Arya, P.K.; Kumar, P.; Negi, B.S.; Jain, N.K.; Sathiaraj, D. Tribological characteristics of additively manufactured $Ti_6Al_4VxCryNi$ alloys. *Mater. Today Commun.* **2024**, *38*, 108113. [CrossRef]
48. Chen, C.; Xie, Y.; Yan, X.; Ahmed, M.; Lupoi, R.; Wang, J.; Ren, Z.; Liao, H.; Yin, S. Tribological properties of Al/diamond composites produced by cold spray additive manufacturing. *Addit. Manuf.* **2020**, *36*, 101434. [CrossRef]
49. Zou, Y.; Tan, C.; Qiu, Z.; Ma, W.; Kuang, M.; Zeng, D. Additively manufactured SiC-reinforced stainless steel with excellent strength and wear resistance. *Addit. Manuf.* **2021**, *41*, 101971. [CrossRef]
50. Zhang, Y.; Liu, Z.; Wang, Y.; Zhai, Y.; Cui, C.; Zhang, Q.; Du, Z.; Yuan, Y.; Wang, X. Study on the role of chromium addition on sliding wear and corrosion resistance of high-manganese steel coating fabricated by wire arc additive manufacturing. *Wear* **2024**, *540*, 205242. [CrossRef]
51. Shang, F.; Xu, Z.; Chen, J.; Chen, L.; Lu, S.; Wang, S.; Jing, X.; Dubovyi, O. Effect of Cr on wear resistance and mechanism of preset-powder laser cladding T15 alloy steel coating. *J. Mater. Res. Technol.* **2024**, *29*, 4991–4999. [CrossRef]
52. Zhu, C.; Fordyce, I.; Sun, S.D.; Annasamy, M.; Fabijanic, D.; Short, K.; Paradowska, A.; Leary, M.; Brandt, M.; Easton, M. Effect of boron addition on the microstructure and wear resistance of laser beam directed energy deposited high chromium white irons. *Wear* **2024**, *546*, 205320. [CrossRef]
53. Shah, R.; Pai, N.; Rosenkranz, A.; Shirvani, K.; Marian, M. Tribological Behavior of Additively Manufactured Metal Components. *J. Manuf. Mater. Process.* **2022**, *6*, 138. [CrossRef]
54. Zhu, Y.; Zou, J.; Chen, X.; Yang, H. Tribology of selective laser melting processed parts: Stainless steel 316 L under lubricated conditions. *Wear* **2016**, *350*, 46–55. [CrossRef]
55. Bartolomeu, F.; Buciumeanu, M.; Pinto, E.; Alves, N.; Carvalho, O.; Silva, F.S.; Miranda, G. 316L stainless steel mechanical and tribological behavior—A comparison between selective laser melting, hot pressing and conventional casting. *Addit. Manuf.* **2017**, *16*, 81–89. [CrossRef]
56. Yu, T.; Liu, J.; He, Y.; Tian, J.; Chen, M.; Wang, Y. Microstructure and wear characterization of carbon nanotubes (CNTs) reinforced aluminum matrix nanocomposites manufactured using selective laser melting. *Wear* **2021**, *476*, 203581. [CrossRef]
57. Jeyaprakash, N.; Yang, C.H.; Ramkumar, K.R. Correlation of Microstructural Evolution with Mechanical and Tribological Behaviour of SS 304 Specimens Developed Through SLM Technique. *Met. Mater. Int.* **2021**, *27*, 5179–5190. [CrossRef]
58. Hemachandra, M.; Thapliyal, S.; Adepu, K. A review on microstructural and tribological performance of additively manufactured parts. *J. Mater. Sci.* **2022**, *57*, 17139–17161. [CrossRef]
59. Du, J.; Lu, M.; Fang, J.; Li, W.; Chen, D. Current-carrying friction of Ag coatings by additive manufacturing: Uncovering the role of electric current. *Mater. Res. Lett.* **2024**, *12*, 459–466. [CrossRef]
60. Ren, C.; Chen, K.; Liang, J.; Narayan, R.L.; Ramamurty, U.; Li, J. Microstructural evolution and its influence on the wear resistance of a laser directed energy deposited Ni-based single crystal superalloy. *J. Mater. Sci. Technol.* **2025**, *205*, 127–138. [CrossRef]
61. Attar, H.; Prashanth, K.G.; Chaubey, A.K.; Calin, M.; Zhang, L.C.; Scudino, S.; Eckert, J. Comparison of wear properties of commercially pure titanium prepared by selective laser melting and casting processes. *Mater. Lett.* **2015**, *142*, 38–41. [CrossRef]
62. Bartolomeu, F.; Buciumeanu, M.; Pinto, E.; Alves, N.; Silva, F.S.; Carvalho, O.; Miranda, G. Wear behavior of Ti6Al4V biomedical alloys processed by selective laser melting, hot pressing and conventional casting. *Trans. Nonferrous Met. Soc. China* **2017**, *27*, 829–838. [CrossRef]
63. Bartolomeu, F.; Sampaio, M.; Carvalho, O.; Pinto, E.; Alves, N.; Gomes, J.R.; Silva, F.S.; Miranda, G. Tribological behavior of Ti6Al4V cellular structures produced by Selective Laser Melting. *J. Mech. Behav. Biomed. Mater.* **2017**, *69*, 128–134. [CrossRef] [PubMed]
64. Shen, X.J.; Zhang, C.; Yang, Y.G.; Liu, L. On the microstructure, mechanical properties and wear resistance of an additively manufactured Ti64/metallic glass composite. *Addit. Manuf.* **2019**, *25*, 499–510. [CrossRef]
65. Kim, K.W.; Kale, A.B.; Cho, Y.H.; Park, S.H.; Lee, K.A. Microstructural and wear properties of WC-12Co cemented carbide fabricated by direct energy deposition. *Wear* **2023**, *518*, 204653. [CrossRef]
66. Khan, A.U.; Sadhya, S.; Bharath Kumar, A.; Chatterjee, S.; Madhukar, Y.K. Investigation on dual wire TIG Arc additive manufacturing of IN625 and SS316L FGM for continuous gradient and sandwich structures. *Thin. Wall. Struct.* **2024**, *200*, 111881. [CrossRef]
67. Lei, J.; Liu, G.; Li, H.; Han, H.; Di, R.; Lei, J. Gaussian and circular oscillating laser directed energy deposition of WC/NiCu composites. *Mater. Charact.* **2023**, *204*, 113218. [CrossRef]
68. Yang, Y.; Zhu, Y.; Khonsari, M.M.; Yang, H. Wear anisotropy of selective laser melted 316L stainless steel. *Wear* **2019**, *428*, 376–386. [CrossRef]
69. Grejtak, T.; Jia, X.; Cunniffe, A.R.; Shi, Y.; Babuska, T.F.; Pack, R.C.; Vermaak, N.; Compton, B.G.; Krick, B.A. Whisker orientation controls wear of 3D-printed epoxy nanocomposites. *Addit. Manuf.* **2020**, *36*, 101515. [CrossRef]
70. Afshari, E.; Ghaffari, M.; Vahedi Nemani, A.; Nasiri, A. Effect of heat treatment on microstructure and tribological performance of PH 13-8Mo stainless steel fabricated via wire arc additive manufacturing. *Wear* **2023**, *526*, 204947. [CrossRef]
71. Dong, E.; Chang, T.; Zhao, L.; Xing, Y.; Chen, J.; Chen, M.; Lu, J.; Cheng, J. Laser metal deposition of AlSi10Mg for aeroengine casing repair: Microhardness, wear and corrosion behavior. *Mater. Today Commun.* **2024**, *38*, 108412. [CrossRef]
72. Liu, G.; Du, D.; Wang, K.; Pu, Z.; Zhang, D.; Chang, B. Microstructure and wear behavior of IC10 directionally solidified superalloy repaired by directed energy deposition. *J. Mater. Sci. Technol.* **2021**, *93*, 71–78. [CrossRef]

73. Li, D.; Yin, F.; Wang, X.; Zhu, S.; Han, G. Research Status and Development Trend of Reinforcement Technique of Nickel-based Superalloy. *Surf. Technol.* **2020**, *49*, 105–122.
74. Ren, C.Y.; Lin, S.C.; Chen, K.; Zhang, D.L.; Zou, G.N.; Liang, X.Q.; Luo, S.H.; He, W.F. Microstructure, thermal stability, and wear resistance of single crystal nickel based high-temperature alloys produced by additive manufacturing. *Chin. J. Nonferrous Met.* **2024**, 1–17.
75. Lewis, S.R.; Lewis, R.; Fletcher, D.I. Assessment of laser cladding as an option for repairing/enhancing rails. *Wear* **2015**, *330*, 581–591. [CrossRef]
76. Farfan-Cabrera, L.I.; Reséndiz-Calderón, C.D.; Hernandez-Peña, A.; Campos-Silva, I.; Gallardo-Hernández, E.A.; Contla-Pacheco, A.D. Tribological effects of boriding treatment on a low carbon steel repaired by wire and arc additive manufacturing. *Surf. Coat. Technol.* **2023**, *465*, 129574. [CrossRef]
77. Liu, J.; Bian, H. Microstructure and properties of laser additive repaired TC17 titanium alloy. *Mod. Mach.* **2023**, *6*, 76–81.
78. Alidokht, S.A.; Wu, L.; Bessette, S.; Chromik, R.R. Microstructure and tribology of cold spray additively manufactured multimodal Ni-WC metal matrix composites. *Wear* **2024**, *538*, 205218. [CrossRef]
79. Yang, Y.; Li, X.; Khonsari, M.M.; Zhu, Y.; Yang, H. On enhancing surface wear resistance via rotating grains during selective laser melting. *Addit. Manuf.* **2020**, *36*, 101583. [CrossRef]
80. Huang, M.; Chen, P.; Qiao, X. Fretting Wear Characteristics of SLM-Formed 316L Stainless Steel in Seawater. *Lubricants* **2022**, *11*, 7. [CrossRef]
81. Rong, T.; Gu, D. Formation of novel graded interface and its function on mechanical properties of WC_{1-x} reinforced Inconel 718 composites processed by selective laser melting. *J. Alloys Compd.* **2016**, *680*, 333–342. [CrossRef]
82. Gu, D.; Hong, C.; Meng, G. Densification, Microstructure, and Wear Property of In Situ Titanium Nitride-Reinforced Titanium Silicide Matrix Composites Prepared by a Novel Selective Laser Melting Process. *Met. Mater. Trans. A* **2011**, *43*, 697–708. [CrossRef]
83. Gu, D.; Hagedorn, Y.C.; Meiners, W.; Meng, G.; Batista, R.J.S.; Wissenbach, K.; Poprawe, R. Densification behavior, microstructure evolution, and wear performance of selective laser melting processed commercially pure titanium. *Acta. Mater.* **2012**, *60*, 3849–3860. [CrossRef]
84. Kang, N.; Coddet, P.; Liu, Q.; Liao, H.; Coddet, C. In-situ TiB/near α Ti matrix composites manufactured by selective laser melting. *Addit. Manuf.* **2016**, *11*, 1. [CrossRef]
85. Zou, S.; Zhao, Z.; Xu, W.; Ni, X.; Zhang, L.; Wu, W.; Kong, D.; He, X.; Wang, L.; Dong, C. Effects of scanning speeds on the wear behavior of CoCrW alloy fabricated by selective laser melting. *Opt. Laser Technol.* **2022**, *147*, 107652. [CrossRef]
86. Yu, Z.; Xu, Z.; Guo, Y.; Sha, P.; Liu, R.; Xin, R.; Li, L.; Chen, L.; Wang, X.; Zhang, Z.; et al. Analysis of microstructure, mechanical properties, wear characteristics and corrosion behavior of SLM-NiTi under different process parameters. *J. Manuf. Process.* **2022**, *75*, 637. [CrossRef]
87. Qin, H.; Xu, R.; Lan, P.; Wang, J.; Lu, W. Wear Performance of Metal Materials Fabricated by Powder Bed Fusion: A Literature Review. *Metals.* **2020**, *10*, 304. [CrossRef]
88. Liu, J.; Yang, Y.; Wu, H.; Yang, Y.; Ren, Y.; Wang, Q.; Agbedor, S.O.; Wu, X.; Lu, Y.; Zhang, Y.; et al. Wear and corrosion of an additively-manufactured AlMgScZrMn alloy. *Mater. Charact.* **2023**, *200*, 112829. [CrossRef]
89. Huang, G.; He, Y.; Long, S.; Duan, Q.; Chen, H.; Peng, X.; Zhou, L.; Huang, K. Microstructure, compressive performance and wear resistance of pure molybdenum additively manufactured via laser powder bed fusion. *Int. J. Refract. Met. Hard Mater.* **2024**, *123*, 106740. [CrossRef]
90. Bordin, A.; Bruschi, S.; Ghiotti, A.; Bariani, P.F. Analysis of tool wear in cryogenic machining of additive manufactured Ti6Al4V alloy. *Wear* **2015**, *328*, 89–99. [CrossRef]
91. Kurzynowski, T.; Smolina, I.; Kobiela, K.; Kuźnicka, B.; Chlebus, E. Wear and corrosion behaviour of Inconel 718 laser surface alloyed with rhenium. *Mater. Des.* **2017**, *132*, 349–359. [CrossRef]
92. Tripathy, M.; Gaskell, K.; Laureto, J.; Davami, K.; Beheshti, A. Elevated temperature fretting wear study of additively manufactured inconel 625 superalloy. *Addit. Manuf.* **2023**, *67*, 103492. [CrossRef]
93. Xiang, D.; Liu, Y.; Yu, T.; Wang, D.; Leng, X.; Wang, K.; Liu, L.; Pan, J.; Yao, S.; Chen, Z. Review on wear resistance of laser cladding high-entropy alloy coatings. *J. Mater. Res. Technol.* **2024**, *28*, 911–934. [CrossRef]
94. Jiang, G.Y.; Lin, F.B. Study on Bacteriostasis, Wear Resistance and Corrosion Resistance of Laser Additive Ni-Cr-Cu Surface. *Hot Work. Technol.* **2024**, 1–6. [CrossRef]
95. Li, G.J.; Li, J.; Luo, X. Effects of post-heat treatment on microstructure and properties of laser cladded composite coatings on titanium alloy substrate. *Opt. Laser Technol.* **2015**, *65*, 66–75. [CrossRef]
96. Lorusso, M. Tribological and Wear Behavior of Metal Alloys Produced by Laser Powder Bed Fusion (LPBF). In *Friction, Lubrication and Wear*; IntechOpen: London, UK, 2019.
97. Karabulut, Y.; Tascioglu, E.; Kaynak, Y. Heat treatment temperature-induced microstructure, microhardness and wear resistance of Inconel 718 produced by selective laser melting additive manufacturing. *Optik* **2021**, *227*, 163907. [CrossRef]
98. Tascioglu, E.; Karabulut, Y.; Kaynak, Y. Influence of heat treatment temperature on the microstructural, mechanical, and wear behavior of 316L stainless steel fabricated by laser powder bed additive manufacturing. *Int. J. Adv. Manuf. Technol.* **2020**, *107*, 1947. [CrossRef]
99. Zhang, M.; Li, C.; Gao, Q.; Fang, J.; Wu, T.L.; Wang, K.H. The effect of heat treatment on microstructure and properties of laser-deposited TiC reinforced H13 steel matrix composites. *Optik* **2020**, *206*, 164286. [CrossRef]

100. Podgornik, B.; Šinko, M.; Godec, M. Dependence of the wear resistance of additive-manufactured maraging steel on the build direction and heat treatment. *Addit. Manuf.* **2021**, *46*, 102123. [CrossRef]
101. Chen, C.; Yan, K.; Qin, L.; Zhang, M.; Wang, X.; Zou, T.; Hu, Z. Effect of Heat Treatment on Microstructure and Mechanical Properties of Laser Additively Manufactured AISI H13 Tool Steel. *J. Mater. Eng. Perform.* **2017**, *26*, 5577–5589. [CrossRef]
102. Sunay, N.; Kaya, M.; Yılmaz, M.S.; Kaynak, Y. Effects of heat treatment on surface integrity and wear performance of Inconel 718 alloy fabricated by laser powder bed fusion process additive manufacturing under different laser power and scanning speed parameters. *J. Braz. Soc. Mech. Sci. Eng.* **2023**, *45*, 430. [CrossRef]
103. Fonseca, E.B.; Gabriel, A.H.G.; Ávila, J.A.; Vaz, R.F.; Valim, D.B.; Cano, I.G.; Lopes, É.S.N. Fracture toughness and wear resistance of heat-treated H13 tool steel processed by laser powder bed fusion. *Addit. Manuf.* **2023**, *78*, 103862. [CrossRef]